Supplementary Information

Tropospheric ozone change from 1980 to 2010 dominated by equatorward redistribution of emissions

Yuqiang Zhang, Owen R. Cooper, Audrey Gaudel, Anne M. Thompson, Philippe Nédélec, Shin-Ya Ogino, J. Jason West

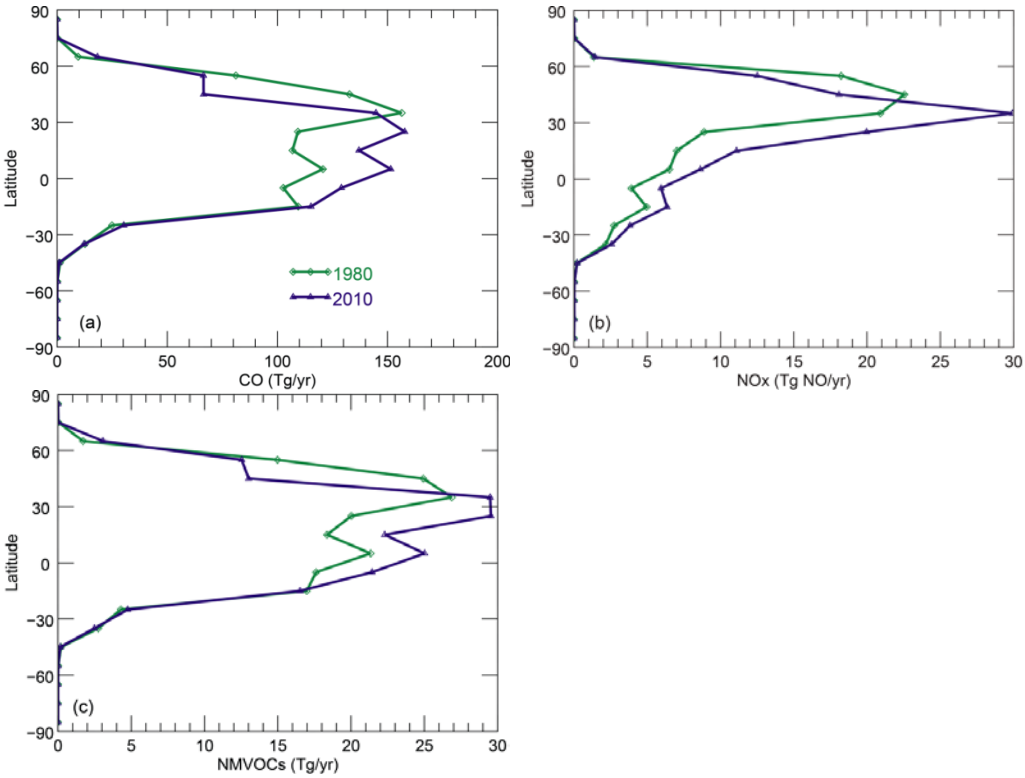

Figure 1. Latitudinal distributions of global anthropogenic emissions in 1980 and 2010, including fire emissions defined as anthropogenic, shown in 10° increments.

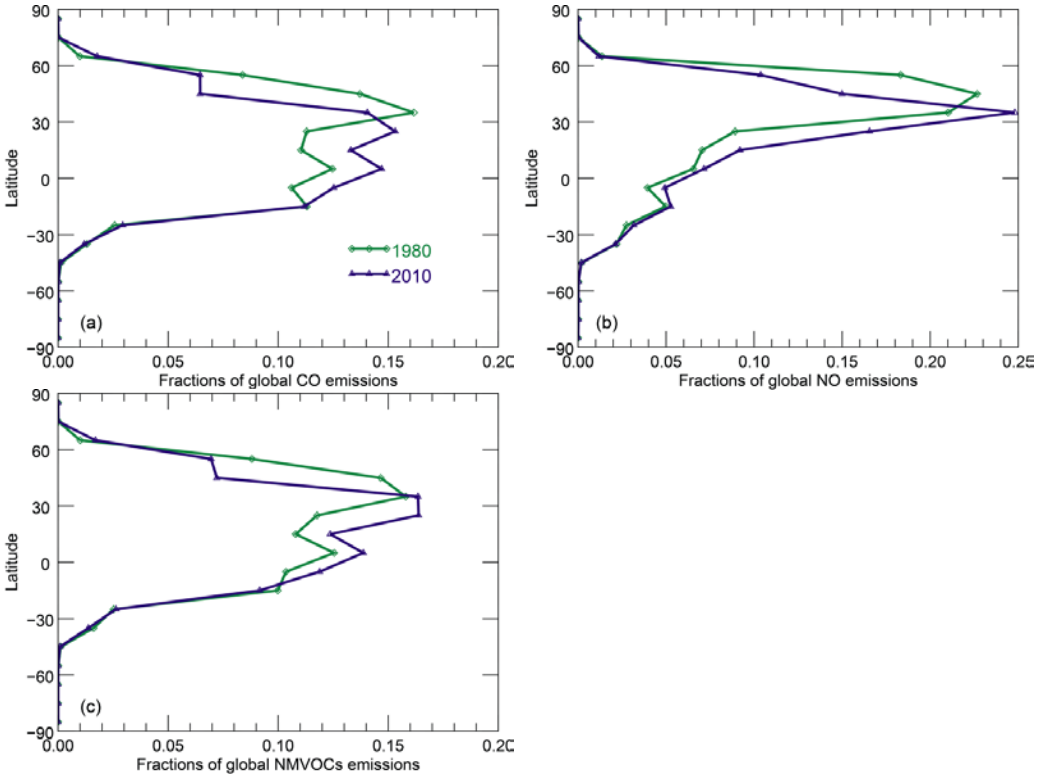

Figure 2. As for Figure 1, but for the emission fractions of global total emissions for each latitudinal band.

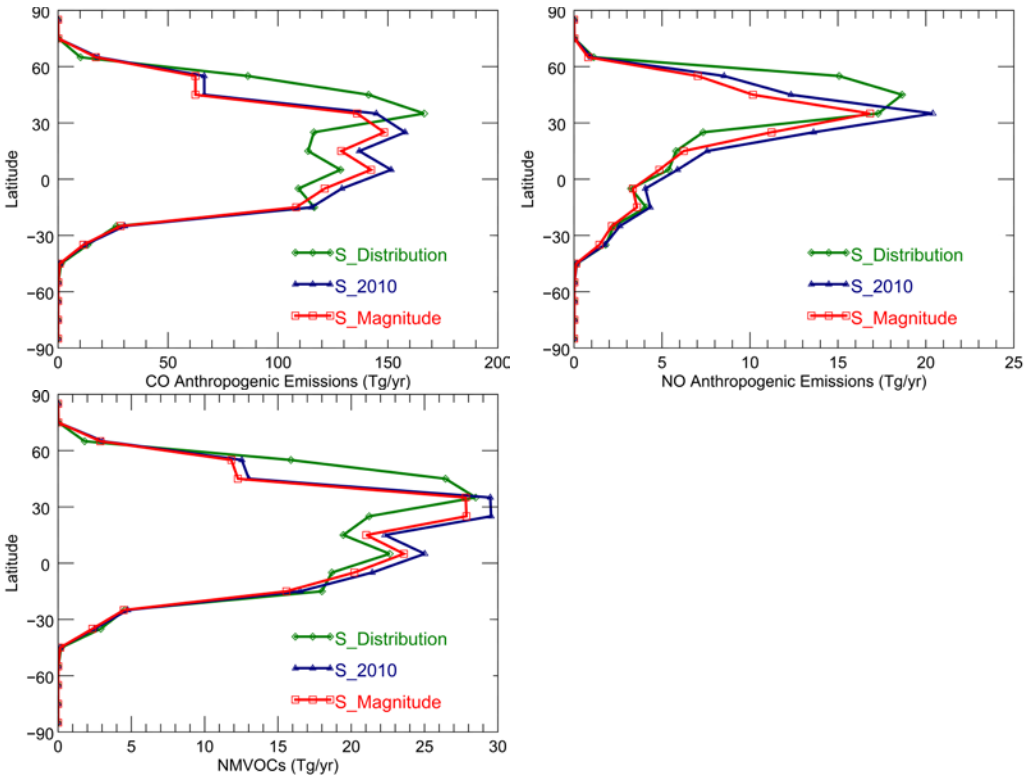

Figure 3. Latitudinal distributions of global anthropogenic emissions in S_2010 and the S_Magnitude and S_Distribution scenarios, including fire emissions defined as anthropogenic, shown in 10° increments.

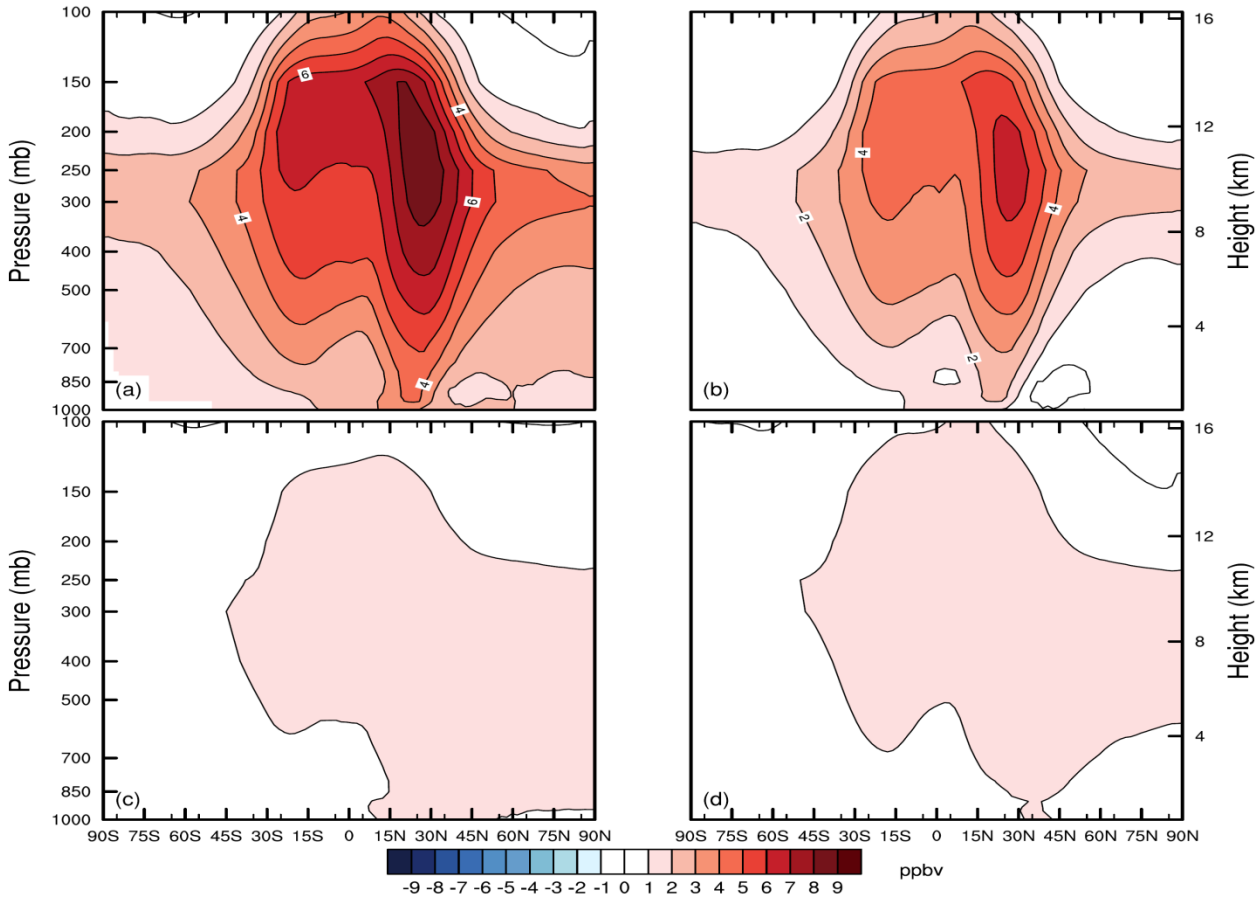

Figure 4. Zonal annual average O_3 change, as in Figure 3 of the main paper, but expressed as changes in mixing ratio (ppb). a, Total change from 1980 to 2010. b-d, Influences of changes in the global emissions spatial distribution, the global emissions magnitude, and global CH_4 mixing ratio.

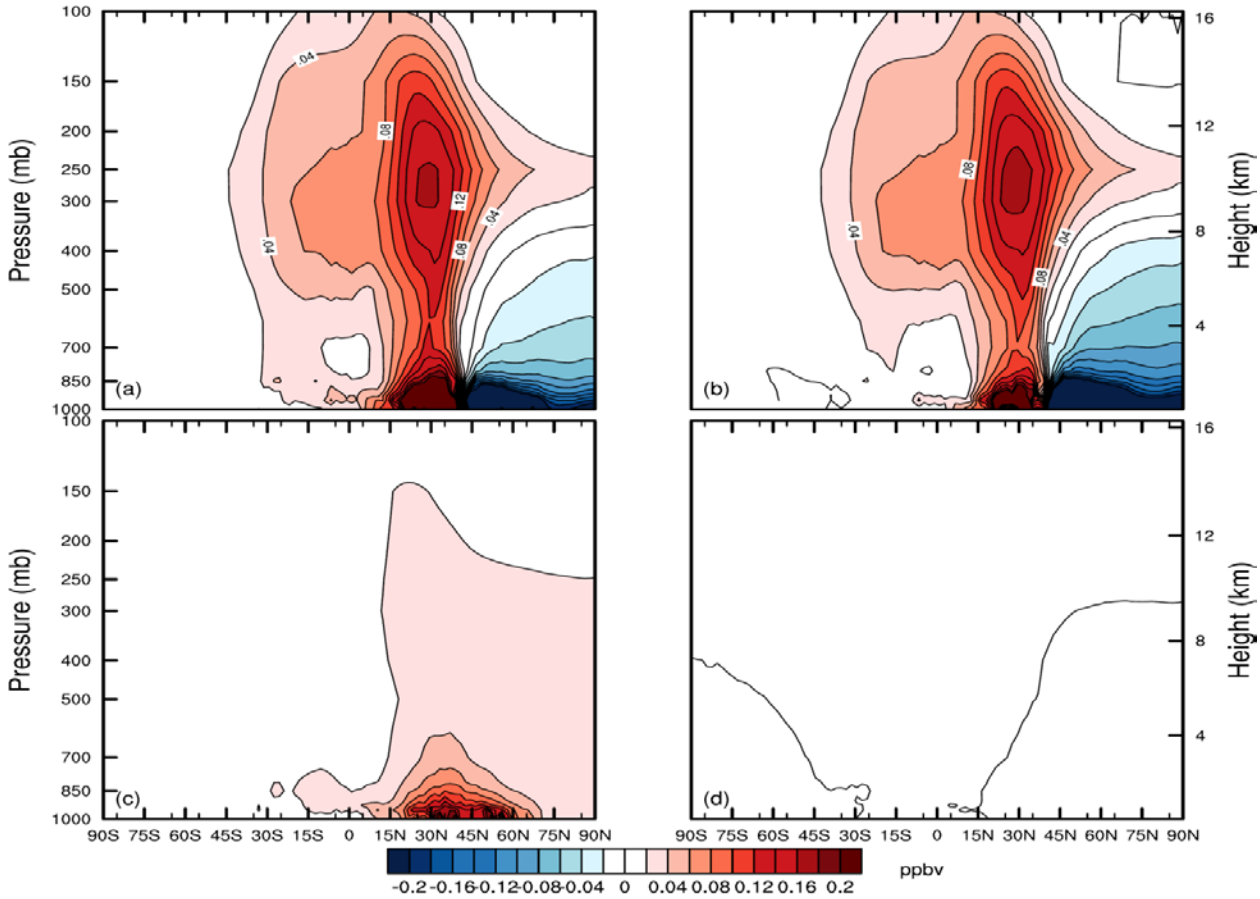

Figure 5. Zonal annual average NO_y change, as in Figure 4 of the main paper, but expressed as changes in mixing ratio (ppb). a, Total changes from 1980 to 2010. b-d, Influences of changes in the global emissions spatial distribution, the global emissions magnitude, and global CH_4 mixing ratio. See Methods for the NO_y definition.

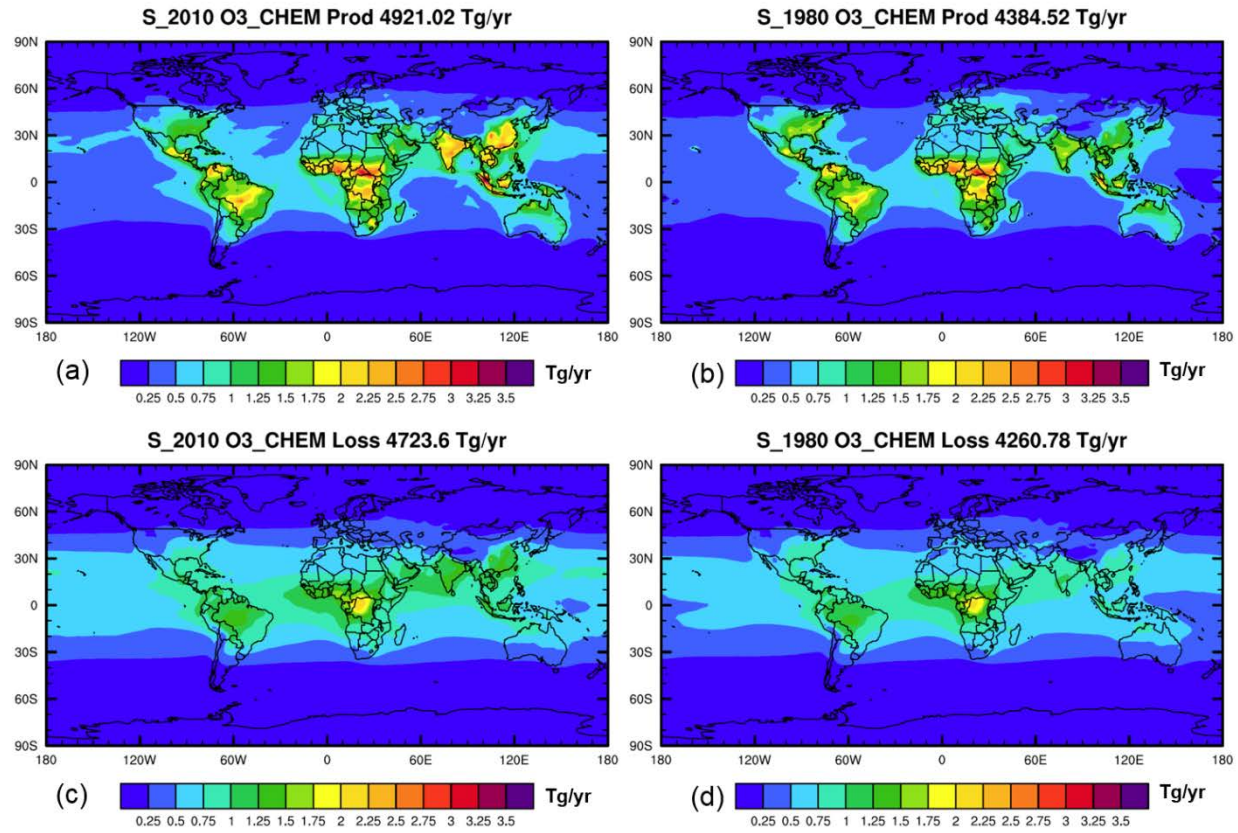

Figure 6. Global O_3 chemical production and loss in 2010 (a, c) and 1980 (b, d), including the O_3 chemical production rate (P_{O3}, a, b) and O_3 chemical loss rate (L_{O3}, c, d).

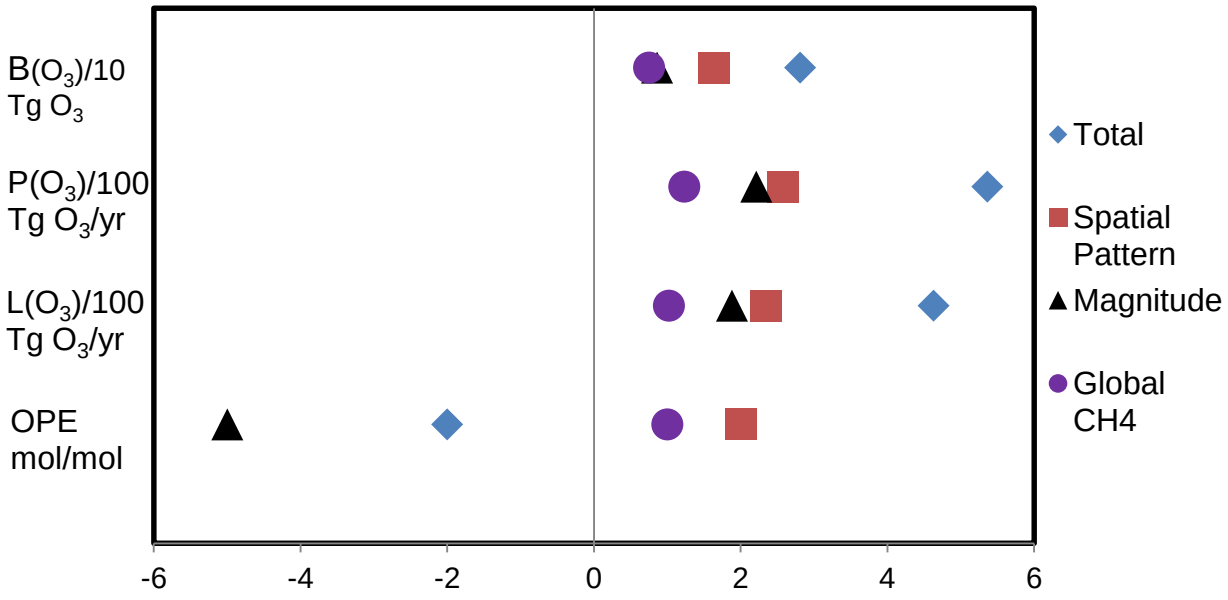

Figure 7. Tropospheric O_3 budget from the different simulations shown as changes relative to S_2010 (Total = S_2010 – S_1980, etc.), for global annual mean tropospheric O_3 burden ($B_{O3}/10$), global annual O_3 chemical production ($P_{O3}/100$), global annual O_3 chemical loss ($L_{O3}/100$), and the global O_3 production efficiency (OPE, mol/mol, defined as the gross O_3 chemical production (P_{O3}) per NO_x emitted (Liu et al., 1987).

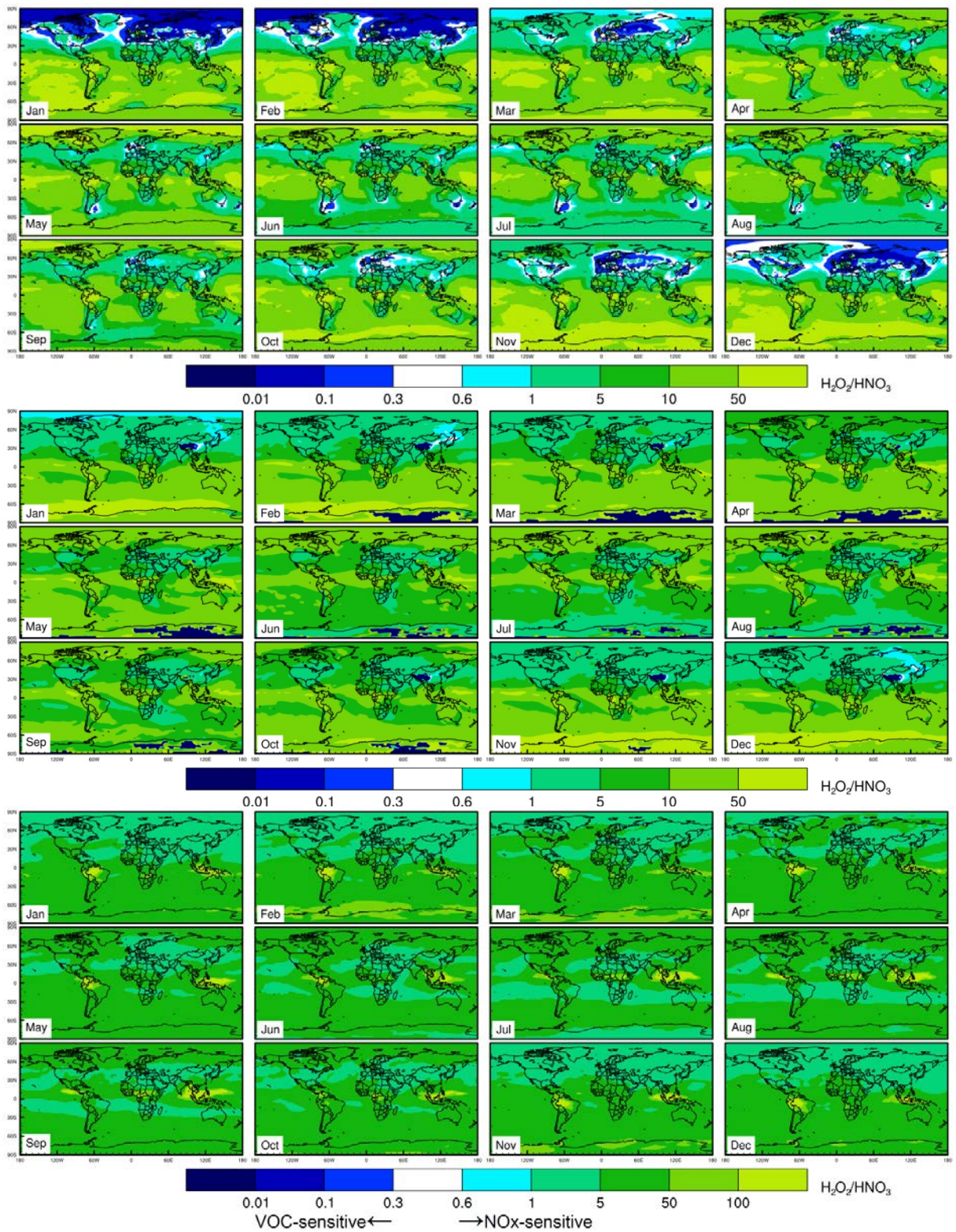

Figure 8. Global distributions of the monthly average surface (top), mid-troposphere (750 hPa, middle) and upper-troposphere (500 hPa, bottom) H_2O_2/HNO_3, with the transition between VOC-sensitive and NO_x-sensitive conditions at roughly 0.3-0.6 (Sillman et al., 1997).

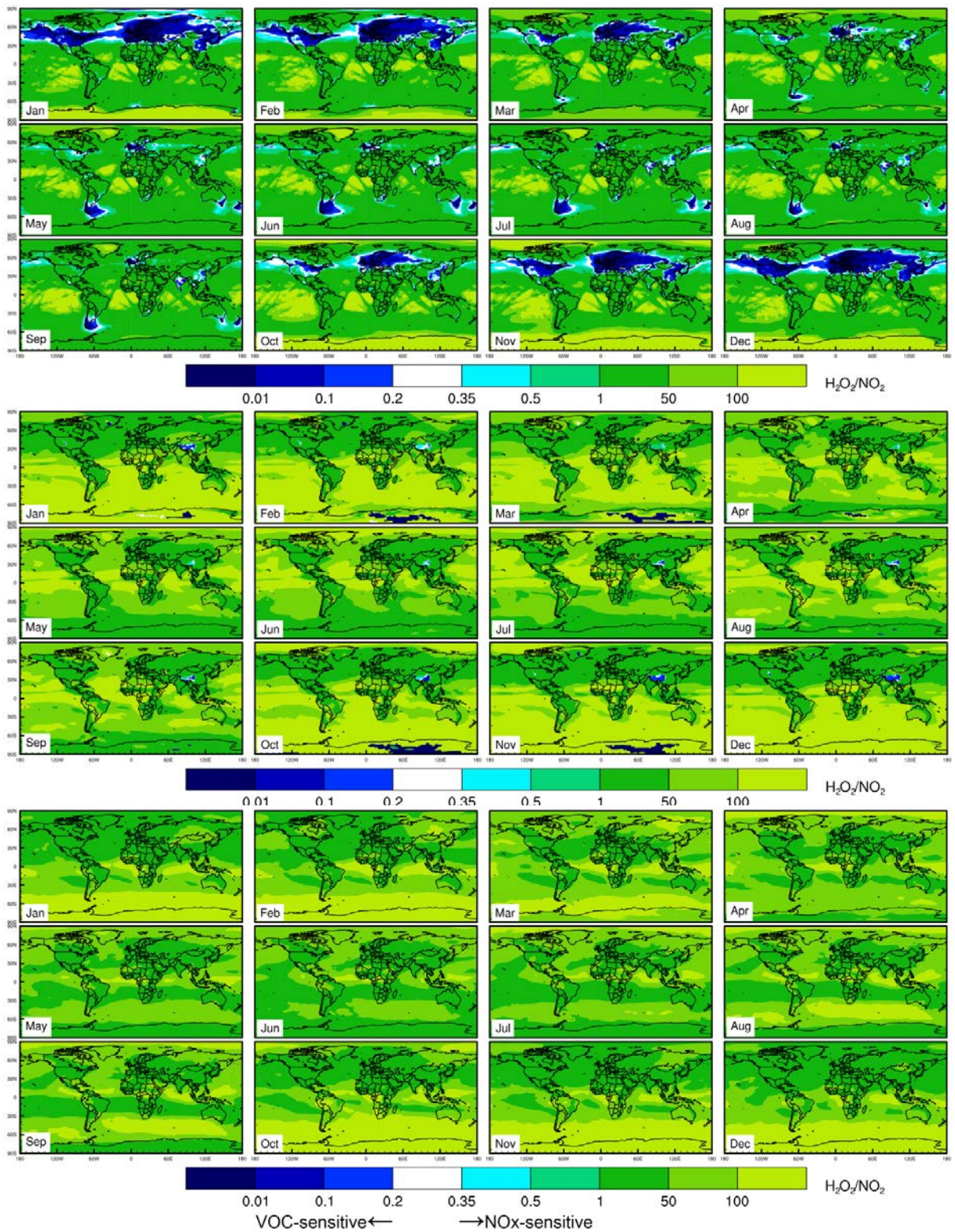

Figure 9. Global distributions of the monthly average surface (top), mid-troposphere (750 hPa, middle) and upper-troposphere (500 hPa, bottom) H_2O_2/NO_2, with the transitions between VOC-sensitive and NO_x-sensitive conditions at roughly 0.2-0.35 (Sillman et al., 1997).

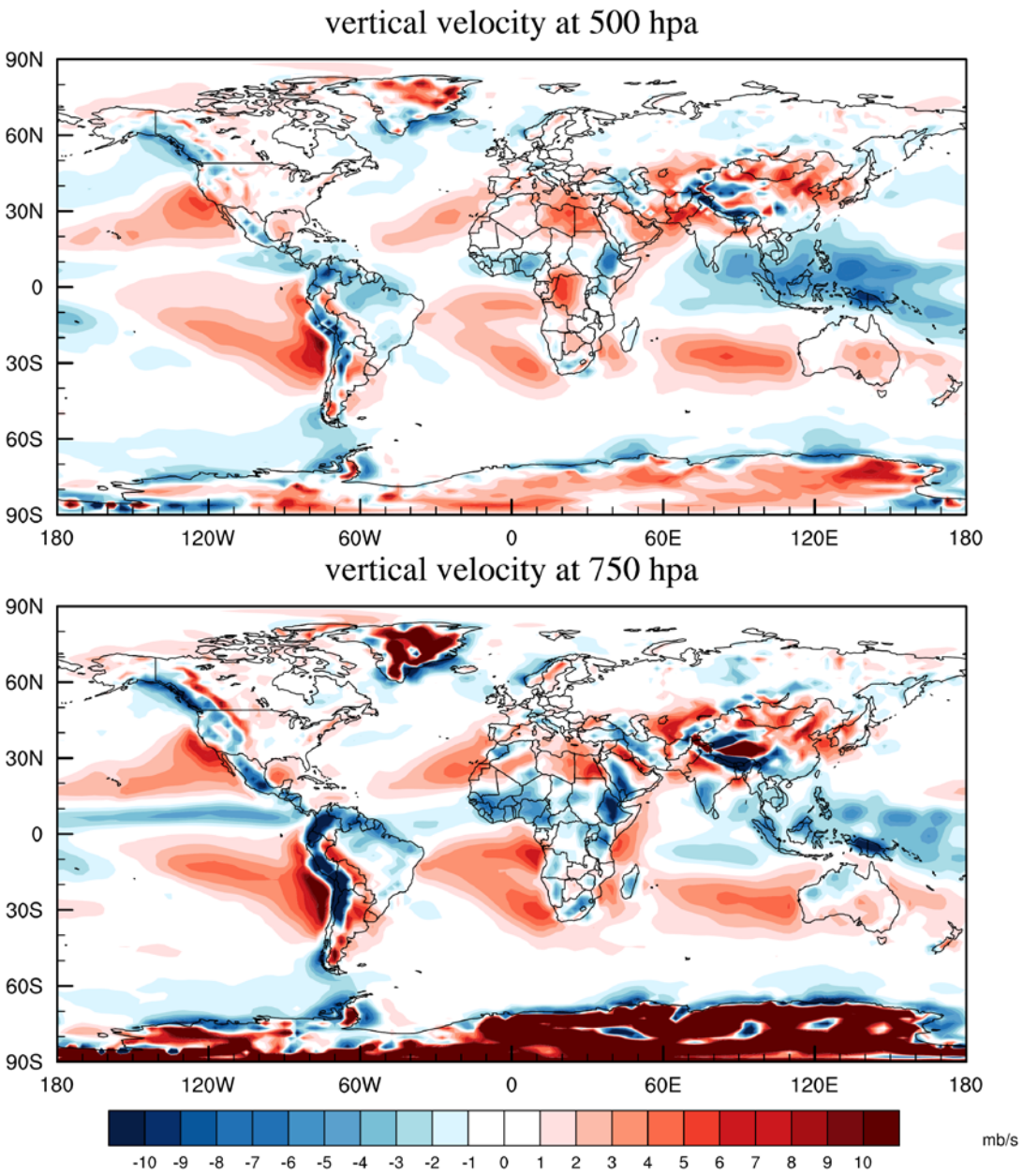

Figure 10. Four-year average vertical velocity at 500 hPa and 750 hPa. Red indicates descending air, and blue indicates ascending air.

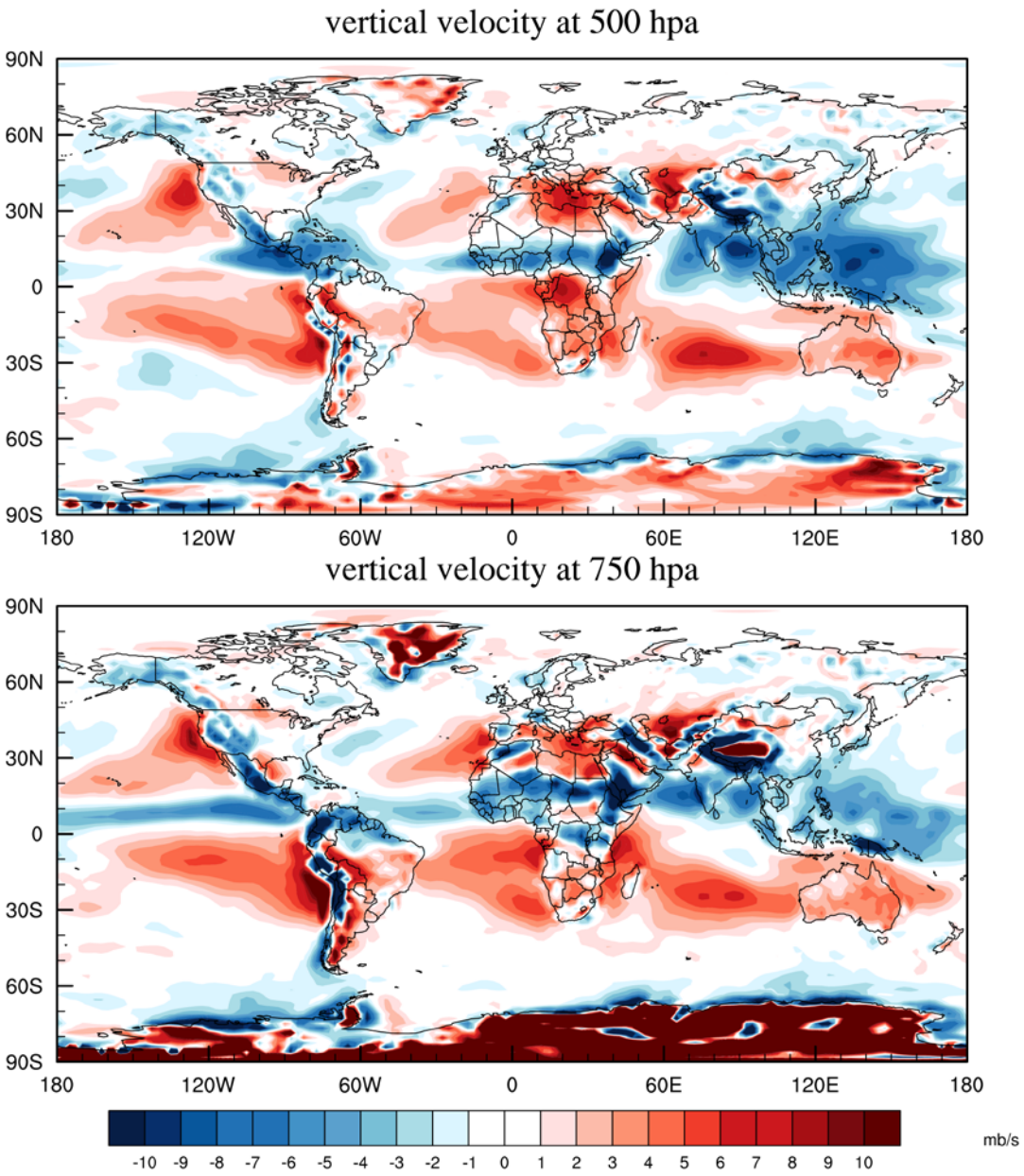

Figure 11. Four-year average of NH-summer (JJA) vertical velocity at 500 hPa and 750 hPa. Red indicates descending air, and blue indicates ascending air.

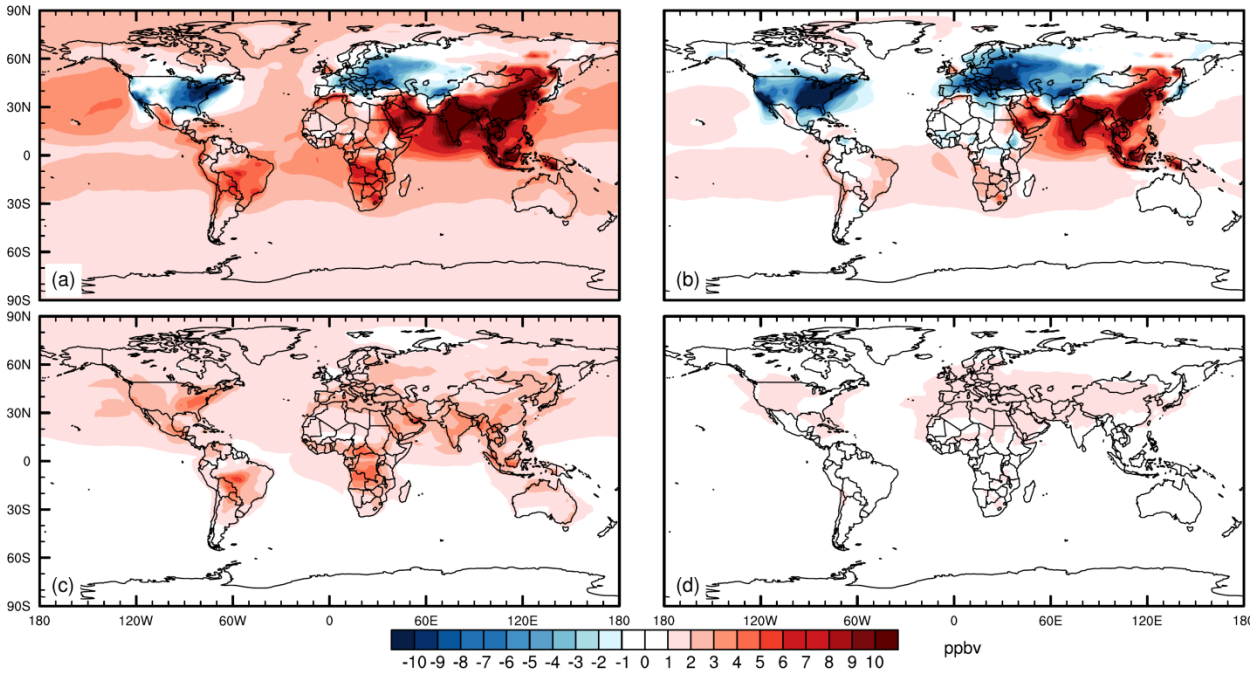

Figure 12. (a) Global surface three-month O_3 season Maximum Daily 8-hr Average O_3 (MDA8) change from 1980 to 2010, and influences of changes in (b) the global emissions spatial distribution, (c) the global emissions magnitude, and (d) global CH_4 mixing ratio.

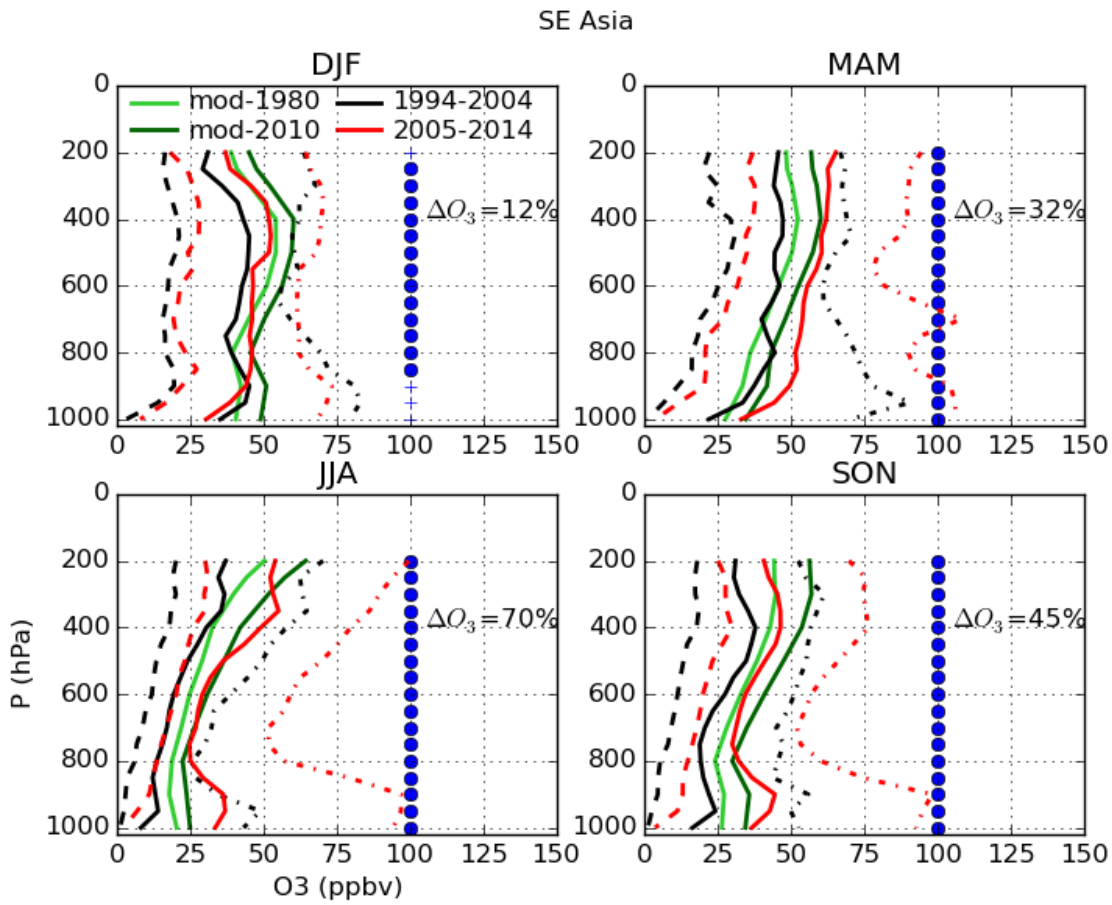

Figure 13. Ozone profiles above Southeast Asia (10°-24°N, 93°-115°E) based on observations from IAGOS commercial aircraft (to and from several airports including Hong Kong, Bangkok, Hanoi, Ho Chi Minh City, and Guangzhou) and SHADOZ ozonesondes from Hanoi, Vietnam. Shown are the 5th (dashed lines), 50th (solid lines) and 95th percentiles (dash-dot lines) for the periods 1994-2004 (black) and 2005-2014 (red). The null hypothesis that the ozone samples in each time period are from the same distribution, for a given layer of the troposphere that was 50 hPa thick, was tested using the Kruskal-Wallis nonparametric one-way analysis of variance test. Layers in which the null hypotheses is rejected at the 95% confidence interval (i.e. there is a significant difference between the samples) are indicted by blue circles. Modeled ozone mixing ratios for the S_1980 and S_2010 simulations (four-year averages) at the same locations as the observations are also shown. The total number of profiles was, for 1994-2004, DJF 182, MAM 213, JJA 206, SON 211, and for 2005-2014, DJF 183, MAM 161, JJA 189, SON 235.

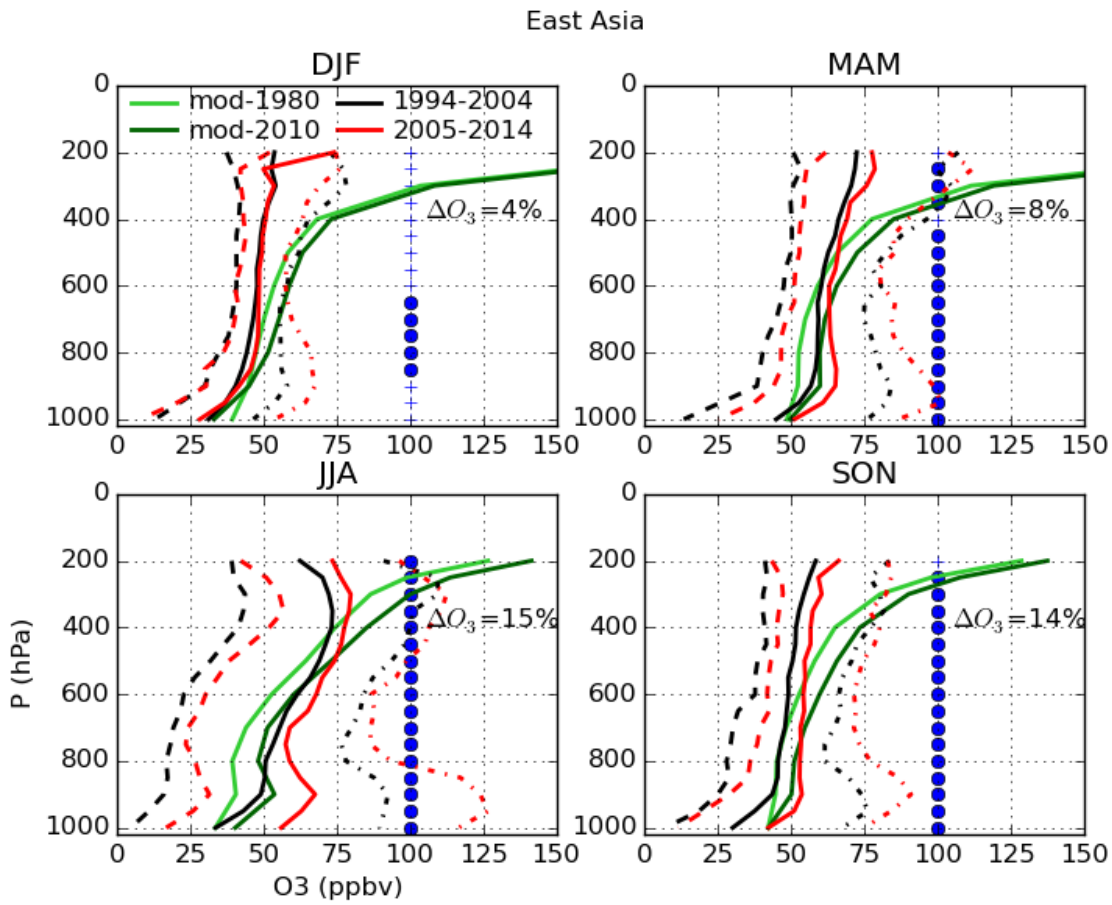

Figure 14. As Figure 13 but for IAGOS observations above northeastern China (30°-43°N, 110°-129°E), to and from several airports including Beijing, Shenyang, Seoul, Zhengzhou, Tianjin, Shanghai, Nanjing and Qingdao). The total number of profiles was, for 1994-2004, DJF 385, MAM 296, JJA 392, SON 304, and for 2005-2014, DJF 208, MAM 291, JJA 221, SON 148.

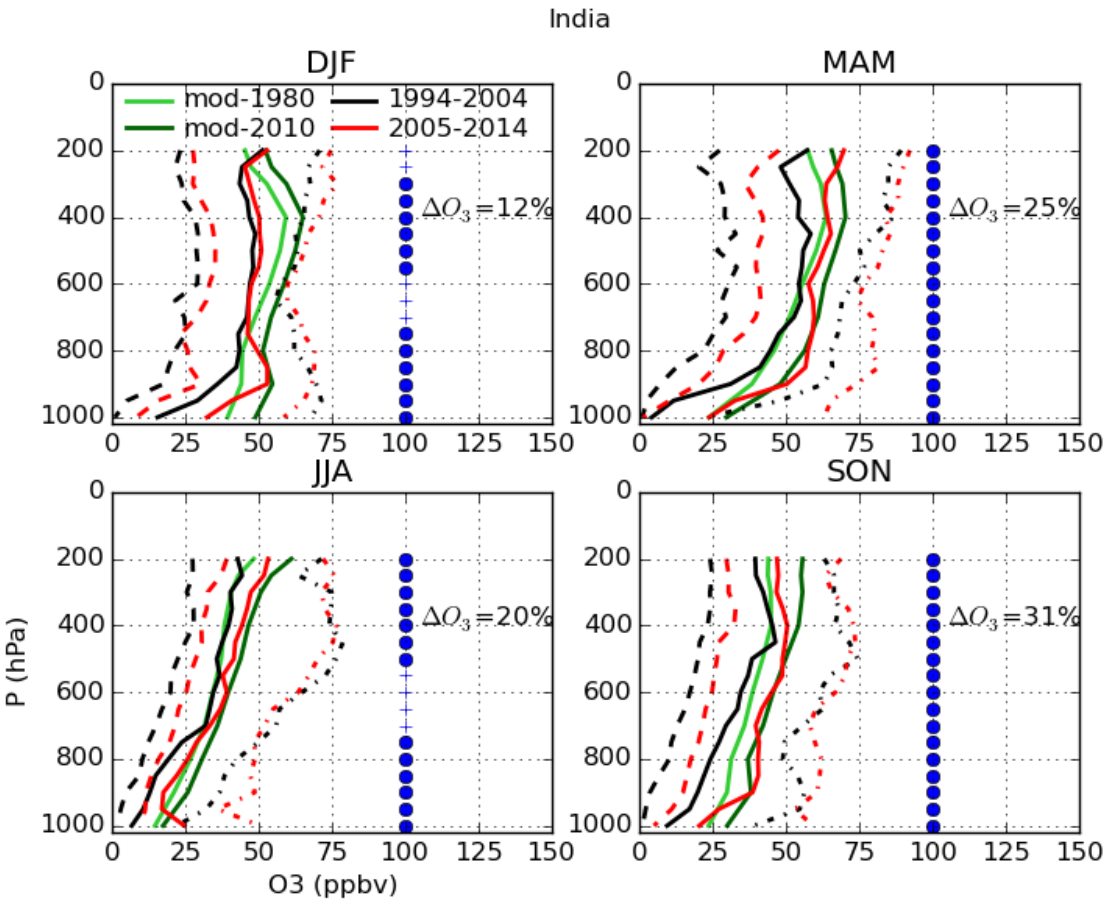

Figure 15. As Figure 13 but for IAGOS observations above southern India (6°-24°N, 70°-89°E, to and from several airports including Hyderabad, Madras, Mumbai, Colombo and Kolkata). The total number of profiles was, for 1994-2004, DJF 84, MAM 91, JJA 107, SON 112, and for 2005-2014, DJF 241, MAM 183, JJA 160, SON 181.

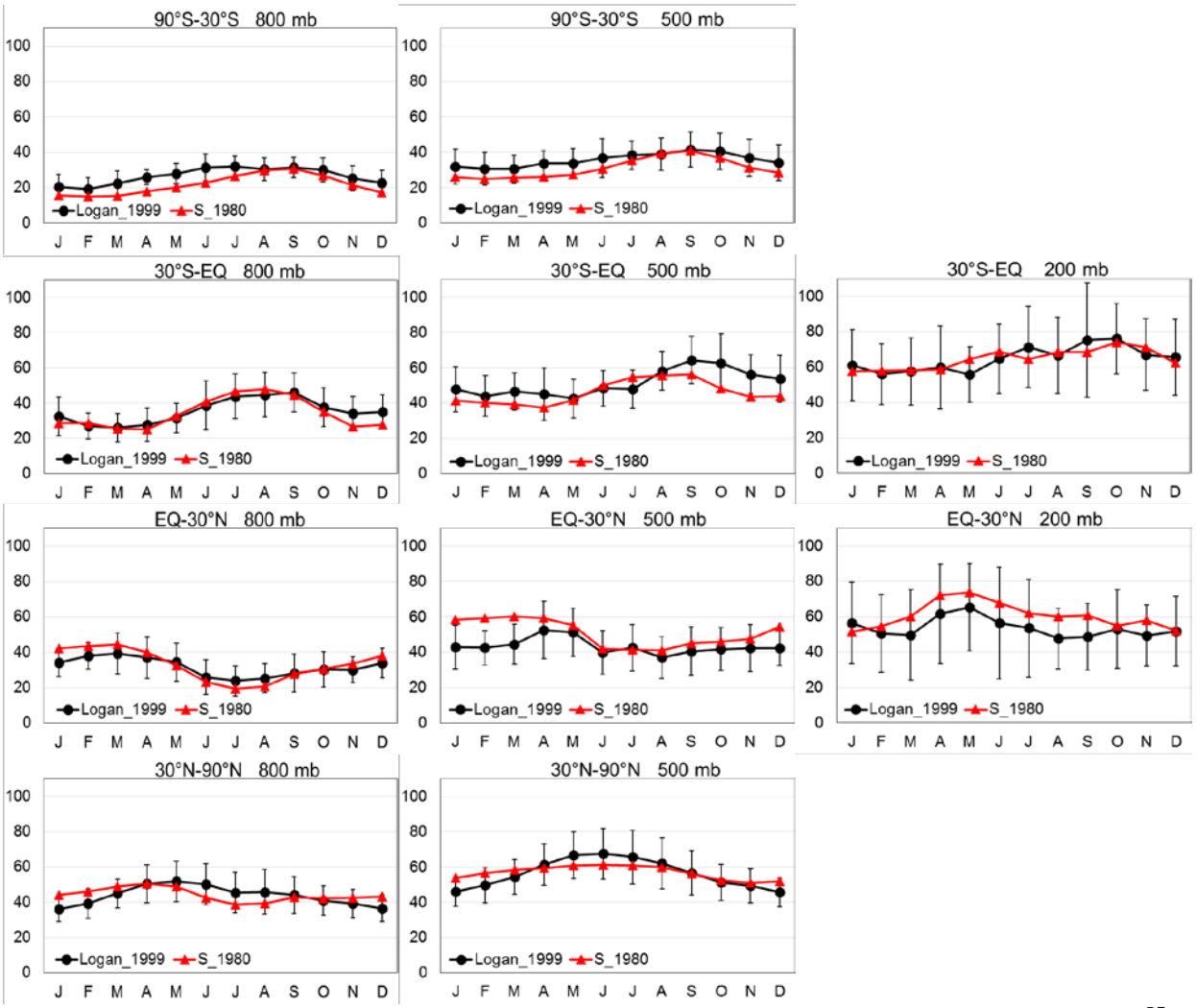

Figure 16. Comparison of seasonal O_3 cycle between ozonesondes observations (Logan et al.[25]) (black circle) and the four-year average for the S_1980 simulation (red triangle). The model was sampled at ozonesonde locations and at three altitudes (800 mb, 500 mb and 200 mb), and then both the model and observational data were grouped into four latitude bands (90°S to 30°S for 5 sites, 30°S to equator for 4 sites, equator to 30°N for 4 sites, and 30°N to 90°N for 18 sites). Observations from (Logan et al.[25]) range between 1966 and 1996, but are between 1980 and 1993 at most sites. Error bars on the observations indicate the average interannual standard deviation for each group of stations.

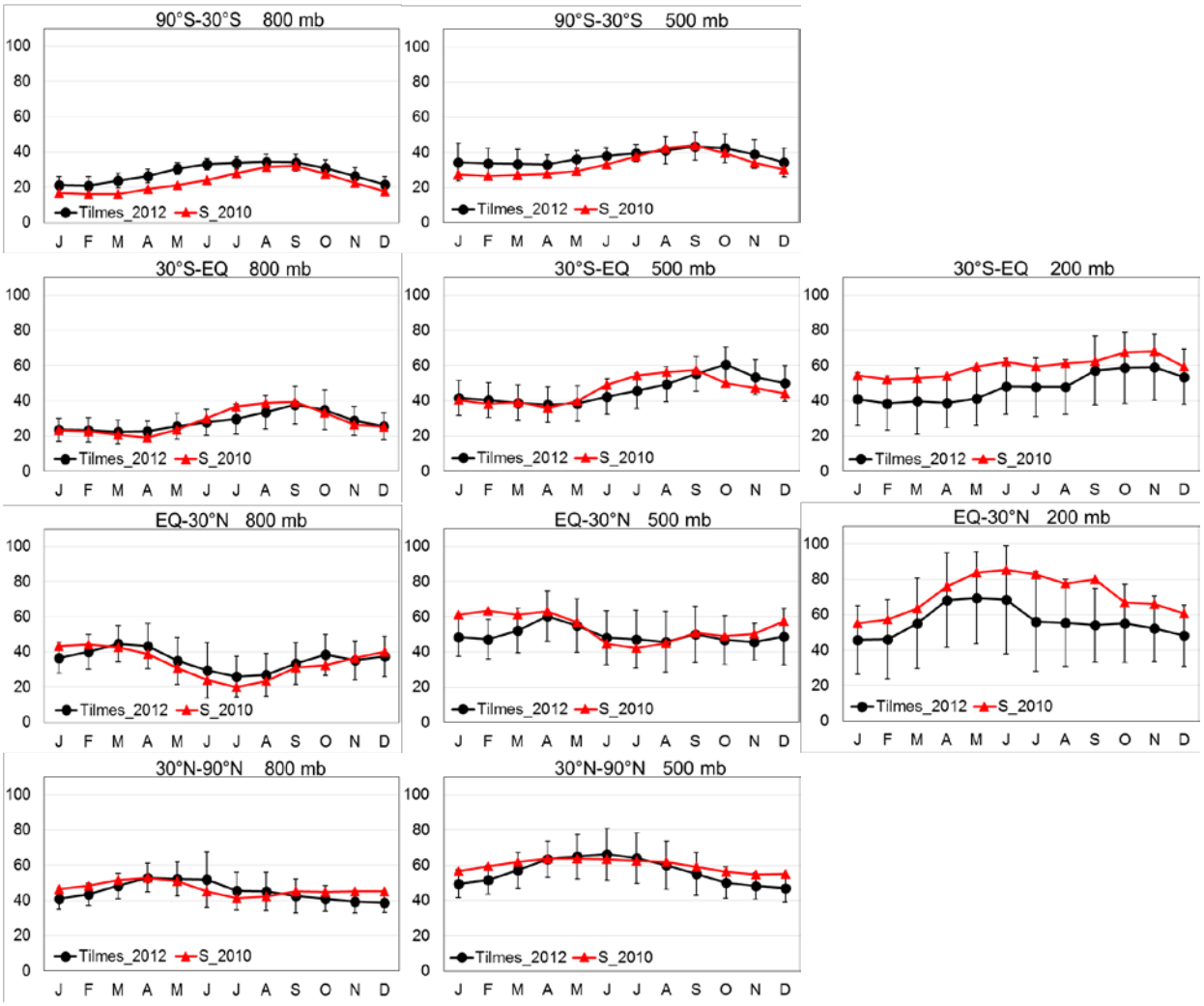

Figure 17. Comparison of seasonal O_3 cycle between ozonesondes observations (Tilmes et al.[26]) (black circle) and the four-year average for the S_2010 simulation (red triangle). The model was sampled at ozonesonde locations and at three altitudes (800 mb, 500 mb and 200 mb), and then both the model and observational data were grouped into four latitude bands (90°S to 30°S for 6 sites, 30°S to equator for 8 sites, equator to 30°N for 4 sites, and 30°N to 90°N for 24 sites). Observations from (Tilmes et al.[26]) are between 1995 and 2011, with some sites covering a smaller range of years. Error bars on the observations indicate the average interannual standard deviation for each group of stations.

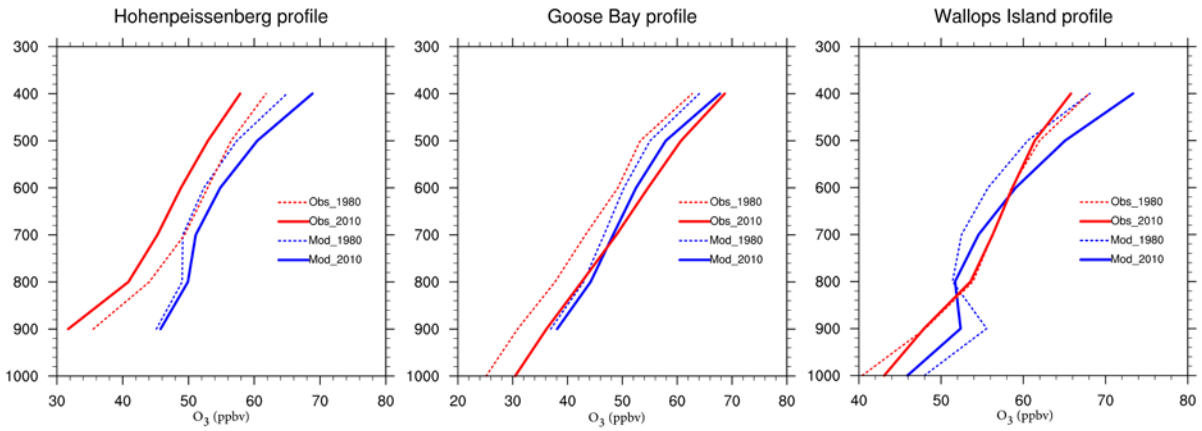

Figure 18. Comparisons of model simulations and ozonesonde observations in 1980 and 2010 at three NH-midlatitude stations (Supplementary Table 8) that have long-term observations. Observations are averaged over ten years from 1976 to 1985 for 1980, and from 2006 to 2015 for 2010, while model results are four year averages.

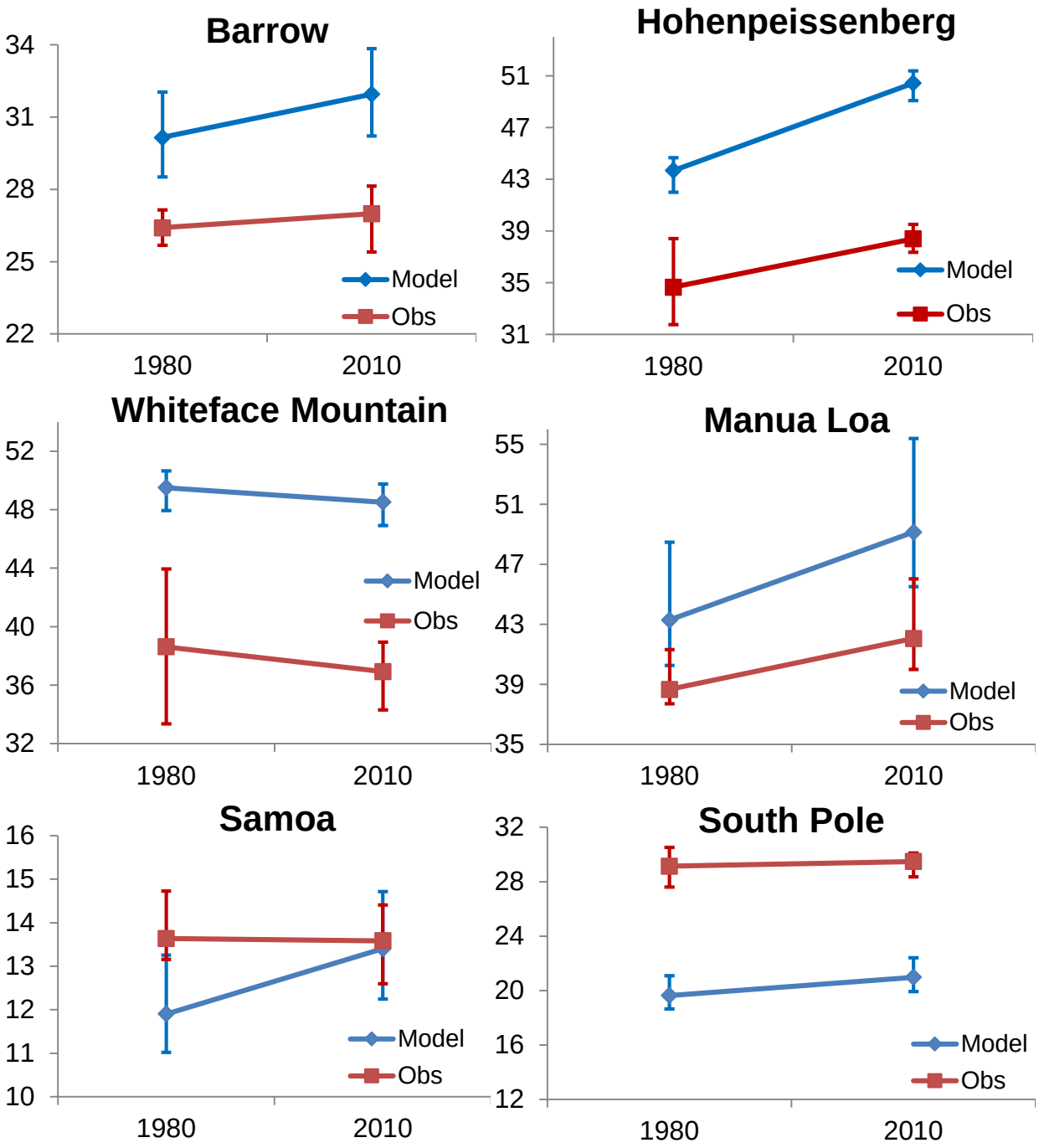

Figure 19. Comparison of the trends of mean O_3 changes (ppbv) from 1980 to 2010 between the model and six long-term rural or remotes sites. All values for both model and observations are four-year averages. The bars are the full range across four annual averages. Observation site means are from 1979 to 1982 for the value in 1980, and from 2009 to 2012 for the value in 2010, except for Hohenpeissenberg which is an average from 2007 to 2010, as more recent observations are not available. Site locations are in Table 5. Four of these sites are elevated (Hohenpeissenberg, Whiteface Mountain, Mauna Loa, and South Pole) and the model was sampled at a vertical level corresponding to the site elevation, with Mauna Loa sampling free tropospheric air.

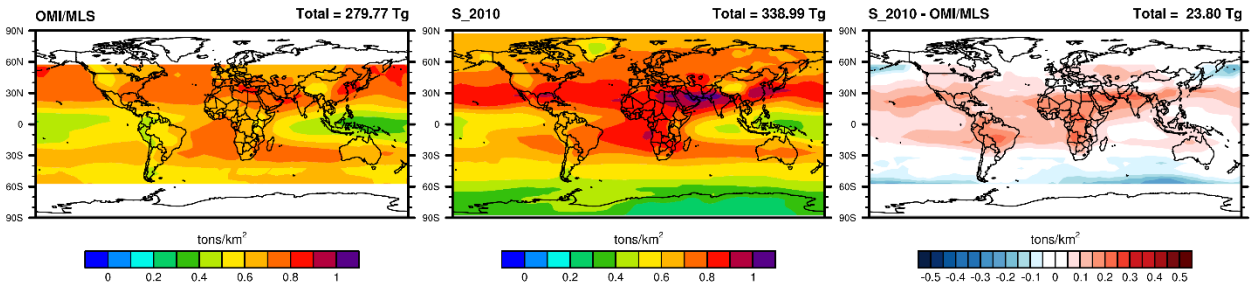

Figure 20. Comparisons of tropospheric column O_3 climatology (tons/km^2) as four-year averages, for (a) OMI/MLS satellite data from 2009 to 2012, (b) the CAM-chem S_2010 simulation, and (c) the differences between CAM-chem and OMI. Tropospheric burdens are shown above each panel, but as there are no OMI/MLS values between 60°N-90°N and 60°S-90°S, the burden shown is between 60°S and 60°N for OMI/MLS and for the model-obs difference, but for the whole world for S_2010.

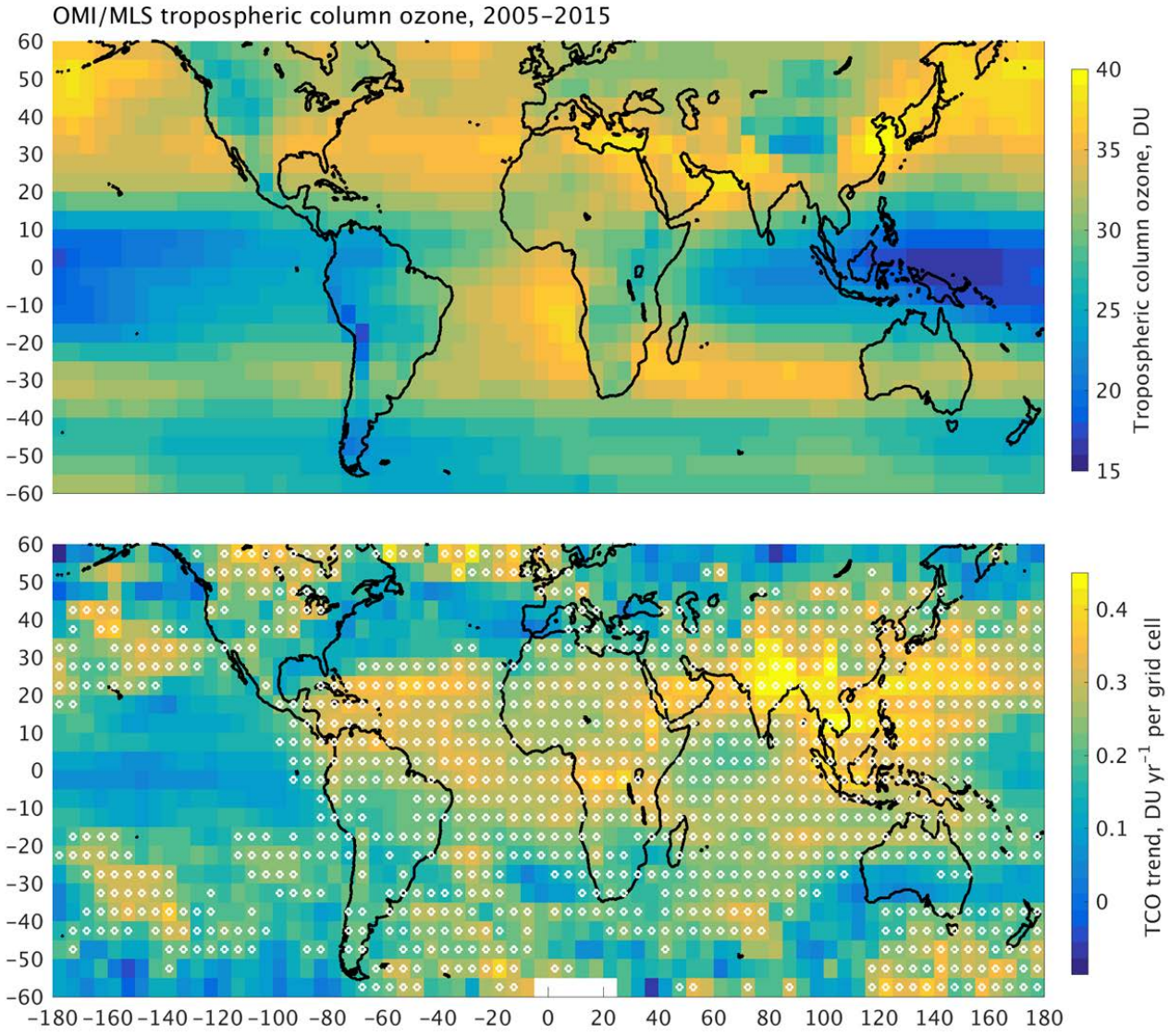

Figure 21. OMI/MLS annual average tropospheric column ozone (top), and 11-year ozone trends from 2004-2015 per 5°x5° grid cell based on least-squares linear fit (bottom). White circles indicate that the ozone trend in that particular grid cell is statistically significant.

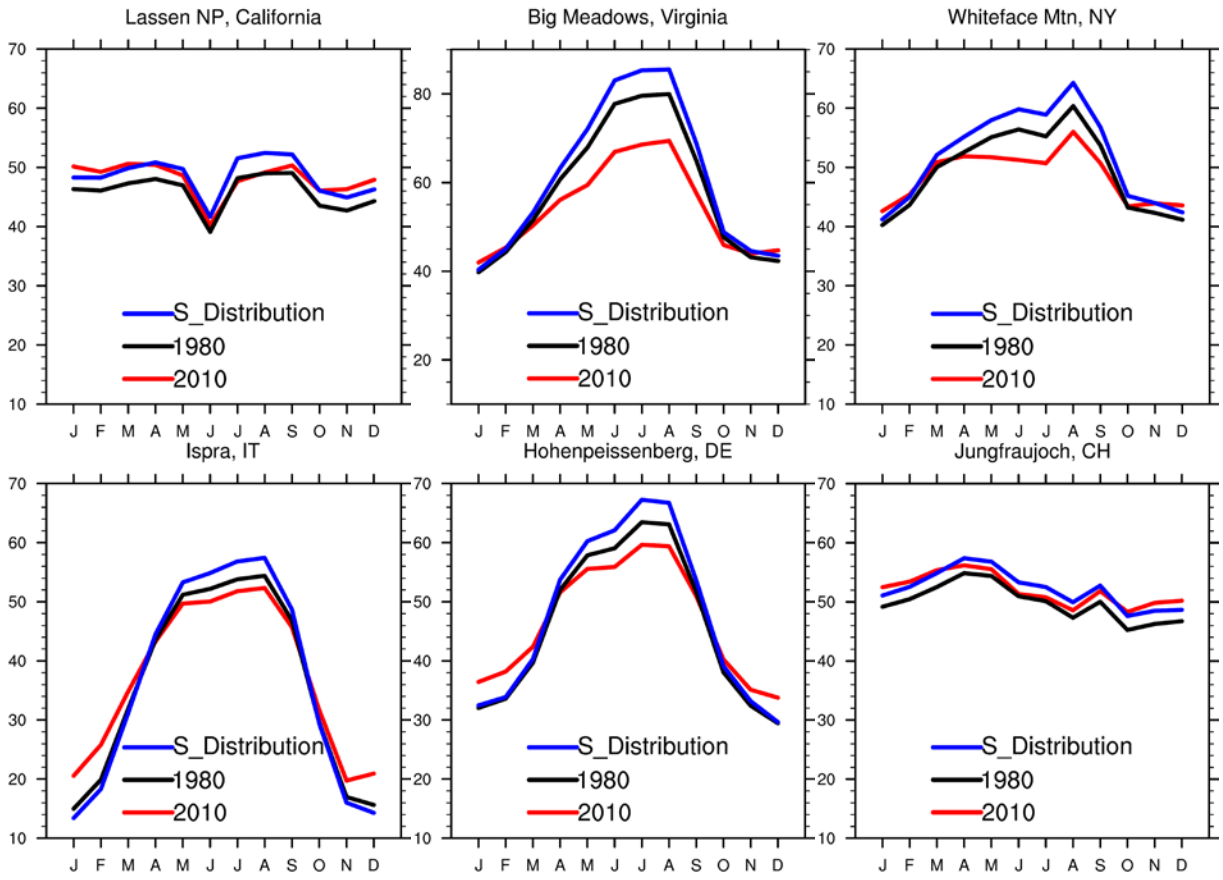

Figure 22. Monthly distributions of modeled ozone (ppb) in 1980 and 2010 and the S_Distribution simulation, for four-year average, at rural observation sites that are observed to experience changes in the seasonal cycle[21,28].

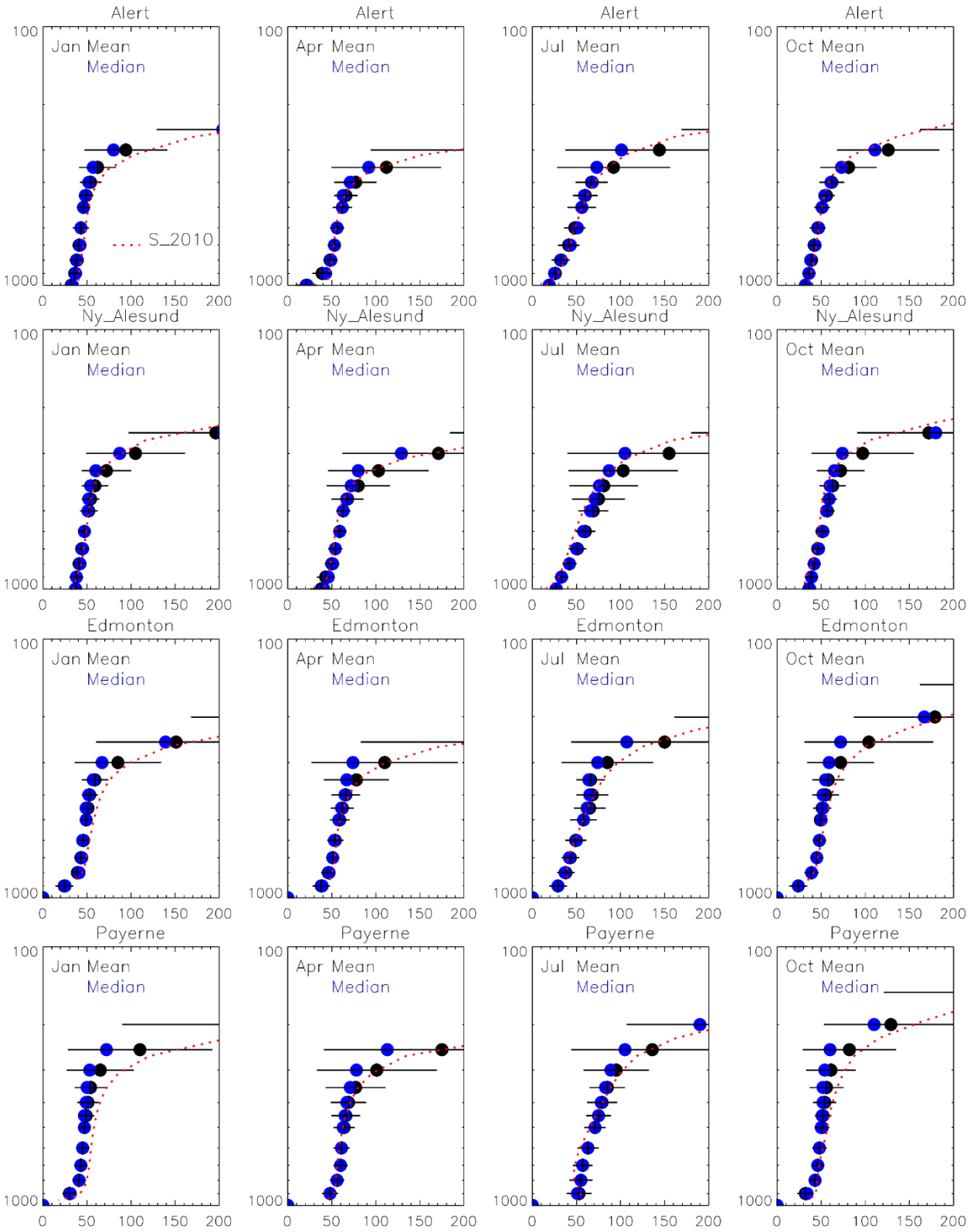
Alert
Jan Mean
Median
S_2010
Alert
Apr Mean
Median
Alert
Jul Mean
Median
Alert
Oct Mean
Median
Ny_Alesund
Jan Mean
Median
Ny_Alesund
Apr Mean
Median
Ny_Alesund
Jul Mean
Median
Ny_Alesund
Oct Mean
Median
Edmonton
Jan Mean
Median
Edmonton
Apr Mean
Median
Edmonton
Jul Mean
Median
Edmonton
Oct Mean
Median
Payerne
Jan Mean
Median
Payerne
Apr Mean
Median
Payerne
Jul Mean
Median
Payerne
Oct Mean
Median
100
1000
0
50
100
150
200

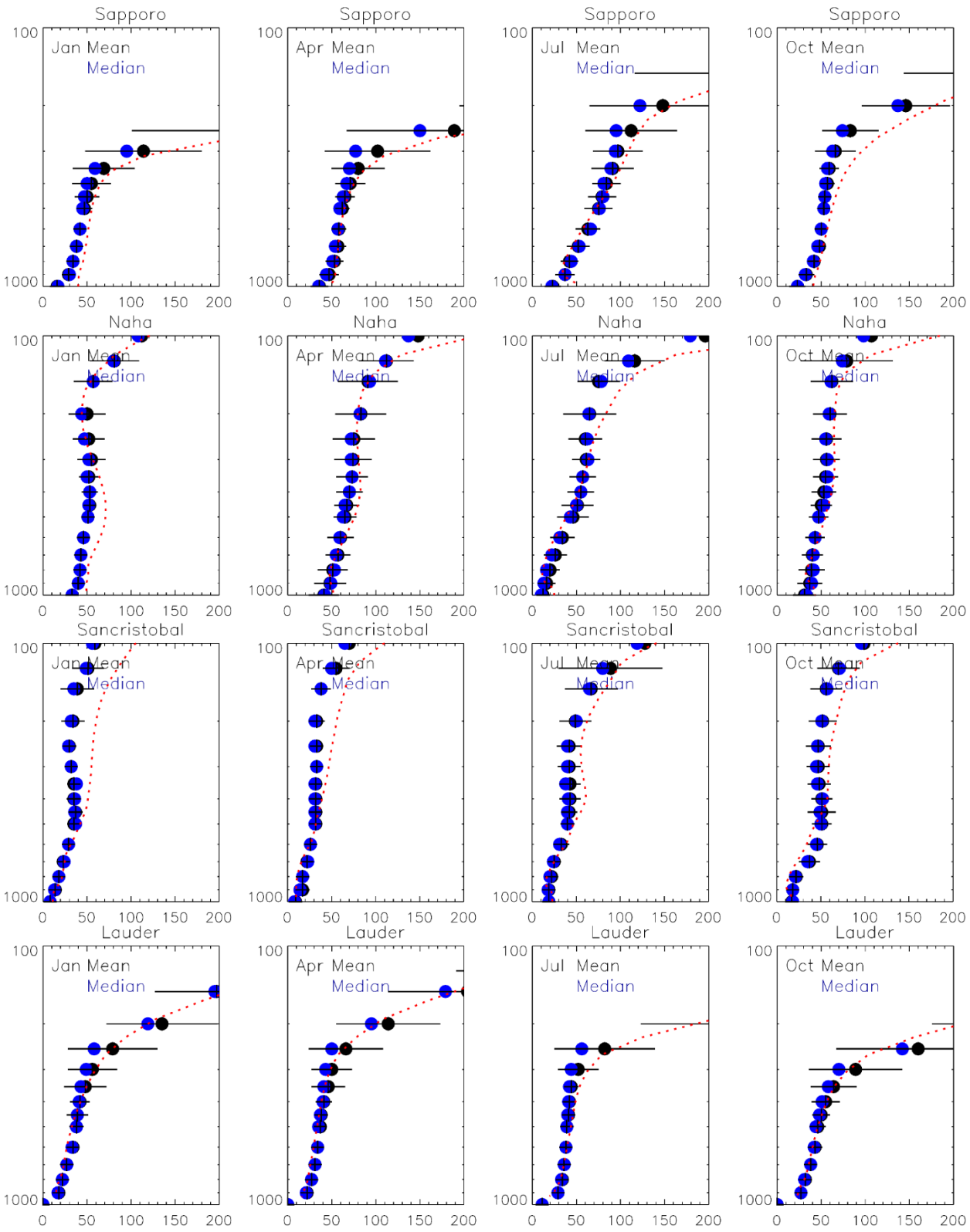
Sapporo
Jan Mean
Median
Sapporo
Apr Mean
Median
Sapporo
Jul Mean
Median
Sapporo
Oct Mean
Median
Naha
Jan Mean
Median
Naha
Apr Mean
Median
Naha
Jul Mean
Median
Naha
Oct Mean
Median
Sancristobal
Jan Mean
Median
Sancristobal
Apr Mean
Median
Sancristobal
Jul Mean
Median
Sancristobal
Oct Mean
Median
Lauder
Jan Mean
Median
Lauder
Apr Mean
Median
Lauder
Jul Mean
Median
Lauder
Oct Mean
Median
100
1000
0
50
100
150
200

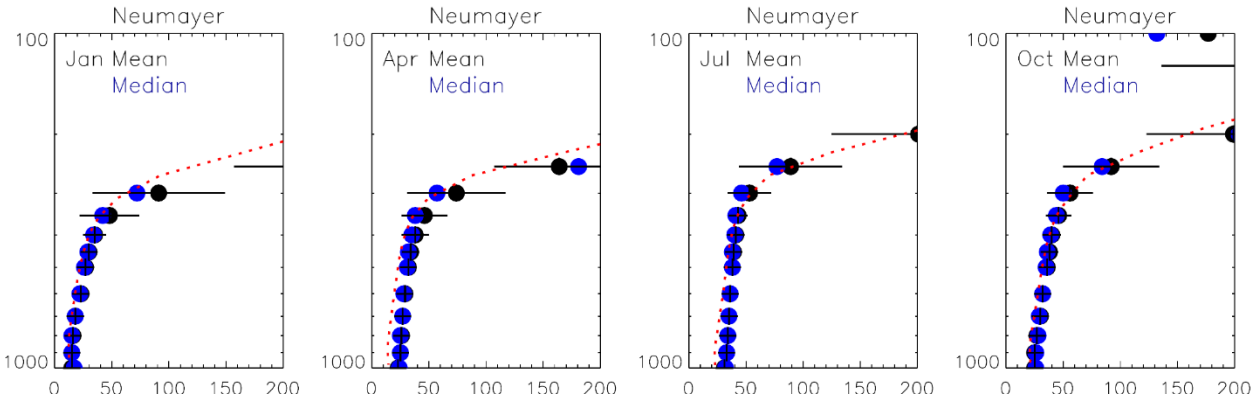

Figure 23. Vertical profile (hPa in the y axis) comparisons of monthly mean tropospheric O_3 mixing ratio (ppbv in the x axis) from the model (red dot) for a four-year average from the S_2010 simulation with the monthly mean (black dot) and median (blue dot) ozonesonde climatology (average of 1995 through 2011, ref. 26) for nine selected ozonesonde stations that are latitudinally representative across the NH and SH, for the months of January, April, July and October.

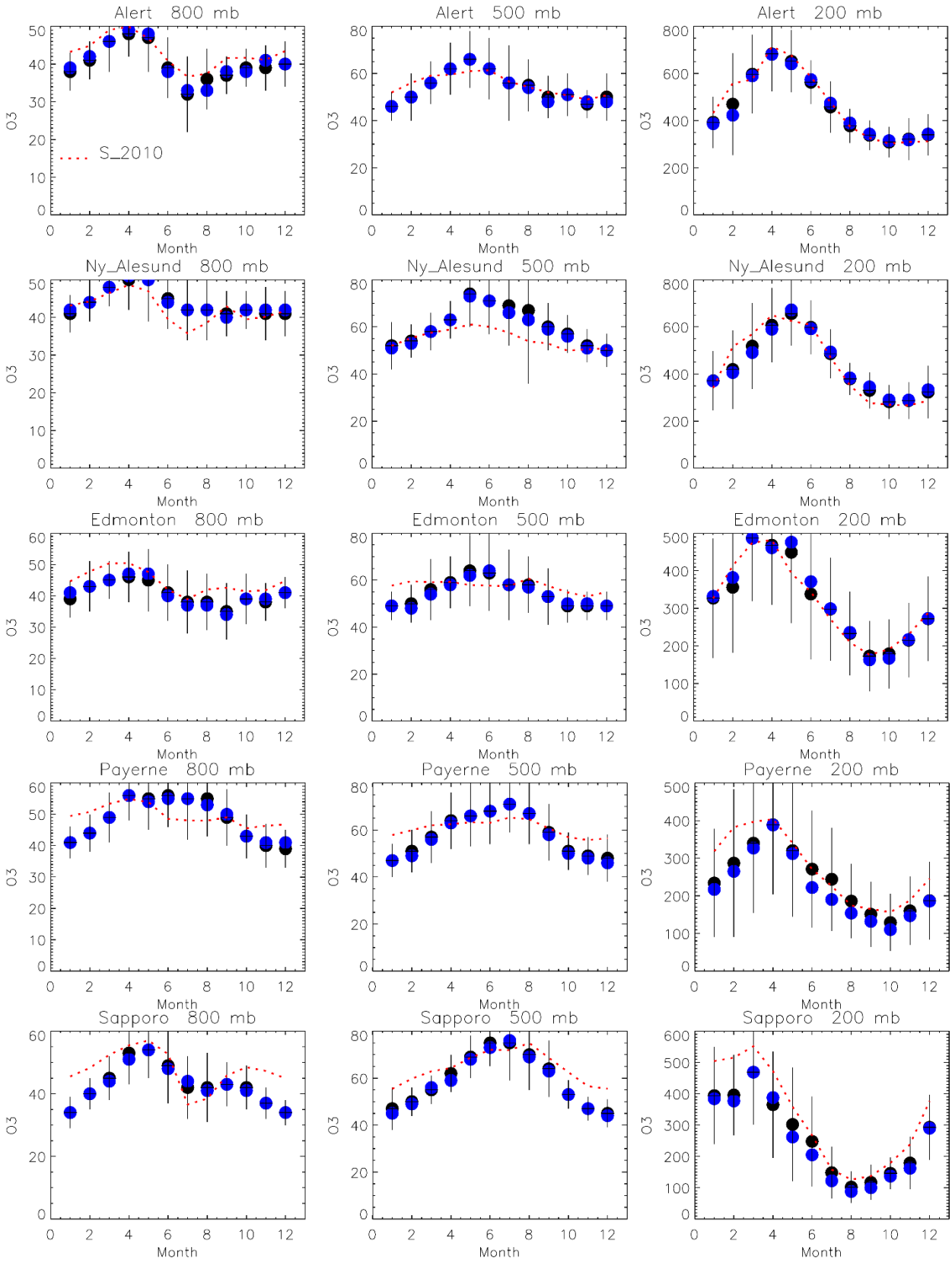
Alert 800 mb
Alert 500 mb
Alert 200 mb
Ny_Alesund 800 mb
Ny_Alesund 500 mb
Ny_Alesund 200 mb
Edmonton 800 mb
Edmonton 500 mb
Edmonton 200 mb
Payerne 800 mb
Payerne 500 mb
Payerne 200 mb
Sapporo 800 mb
Sapporo 500 mb
Sapporo 200 mb
S_2010
O3
Month

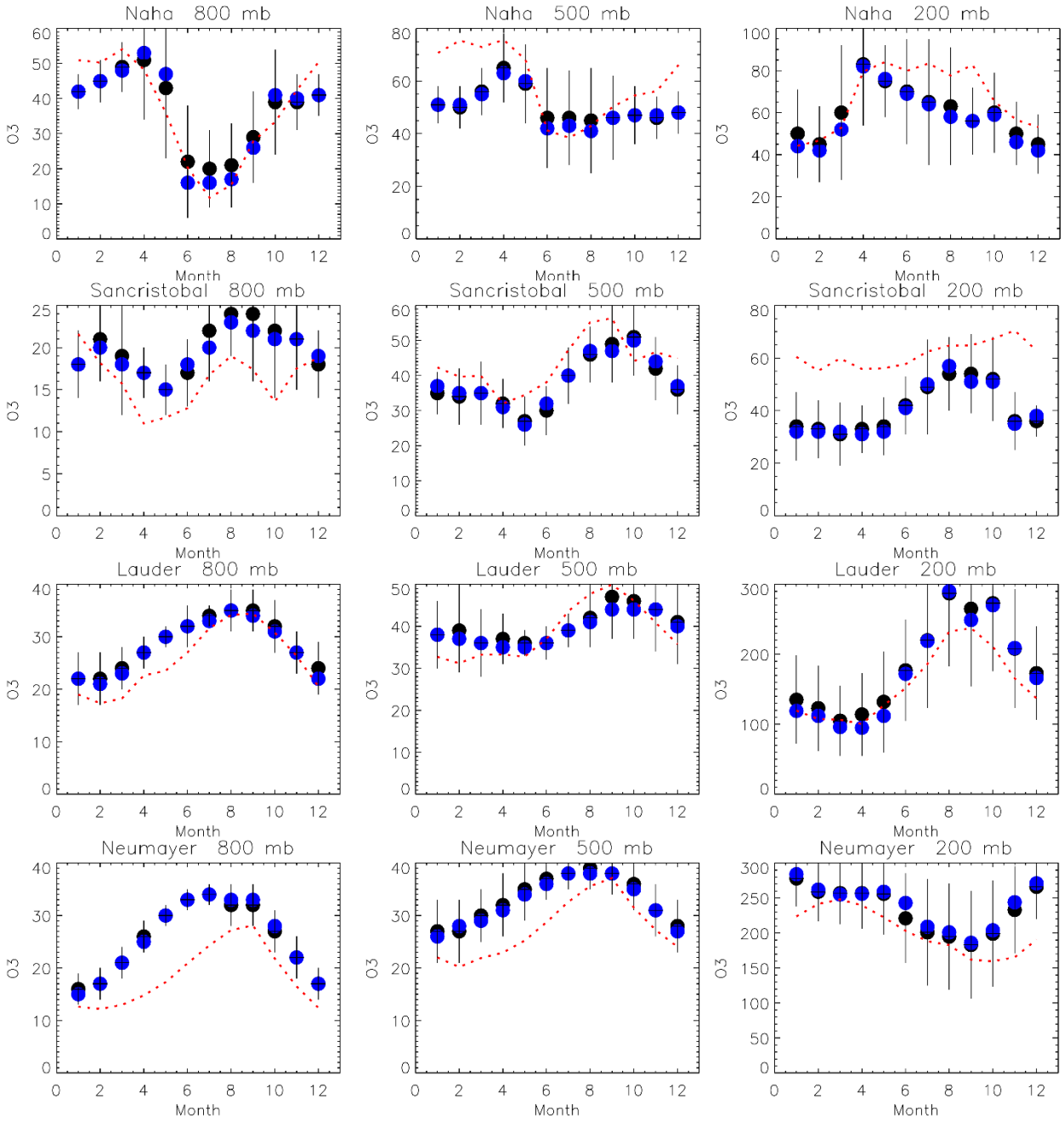

Figure 24. Comparisons of the base simulated monthly mean tropospheric O_3 concentrations from the S_2010 simulation (ppbv in the y axis) for the years 2009-2012 (red dot) with the monthly mean (black dot) and median (blue dot) ozonesonde climatology (averaged over 1995 through 2011, ref. 26) for nine selected ozonesonde stations that are latitudinally representative across the northern and southern hemispheres at altitudes of 800, 500, and 200 hPa.

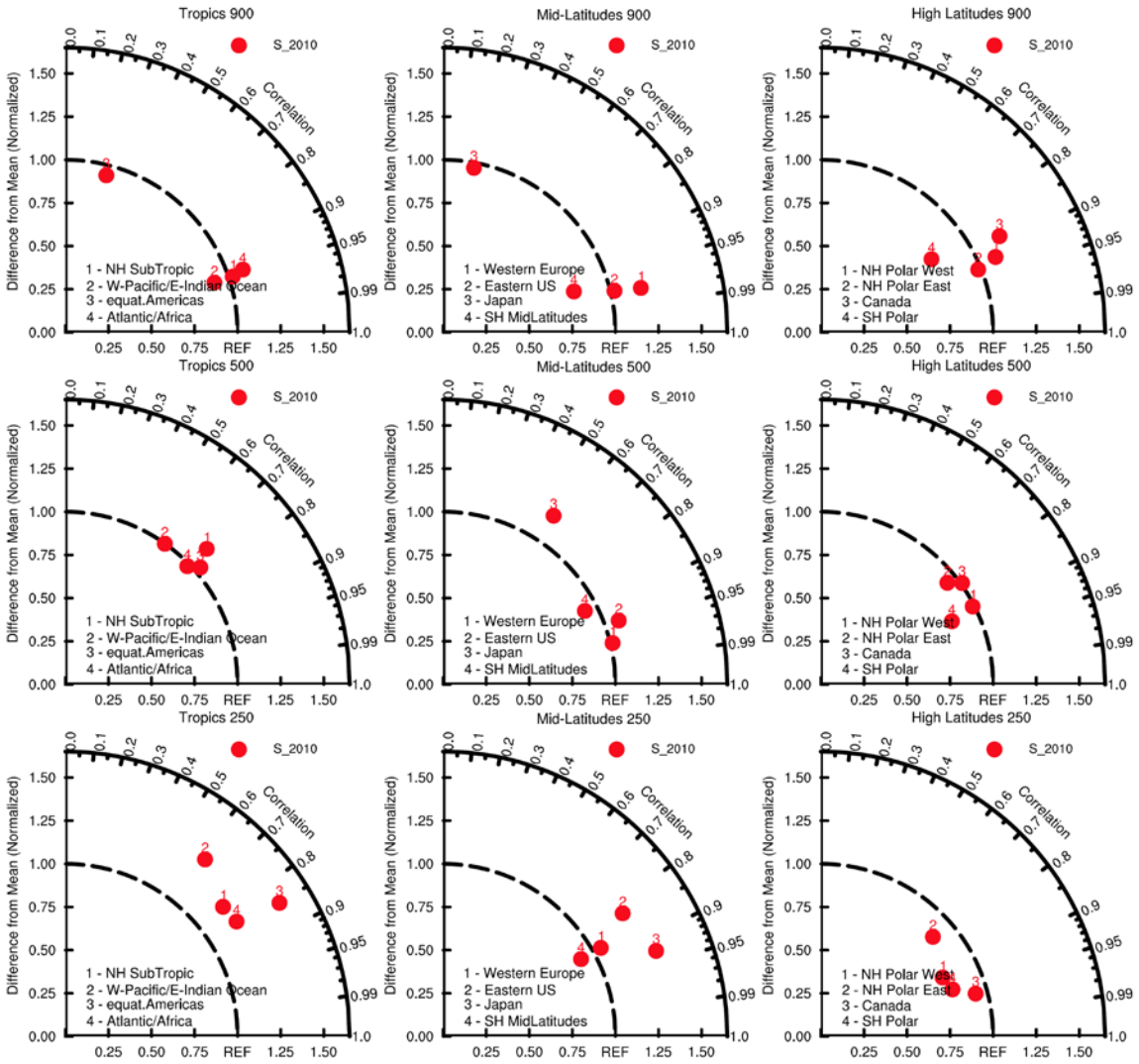

Figure 25. Taylor diagram of comparisons between modeled monthly mean ozone from the S_2010 simulation and ozonesonde climatology data from 1995 to 2011 (as Supplementary Fig. 23 and 24) in the high Tropics (left), mid-latitudes (middle), and high-latitudes (right) for three different altitude levels (900 hPa, 500 hPa and 250 hPa) in the troposphere. The x-axis shows the relative ozone normalized bias of the simulations compared to the observations, whereas the radiant in the y-axis describes the correlation coefficient of seasonal averaged ozone values between simulated and observed values. Numbers indicate different regions as difference in previous studies[26,40]. Left panels: 1—NH Subtropics; 2—W-Pacific/E-India Ocean; 3—equat. America; 4—Altantic/Africa; Middle panels: 1—Western Europe; 2—Eastern US; 3—Japan; 4—SH MidLatitudes; Right panels: 1—NH Polar West; 2—NH Polar East; 3—Canada; 4—SH Polar.

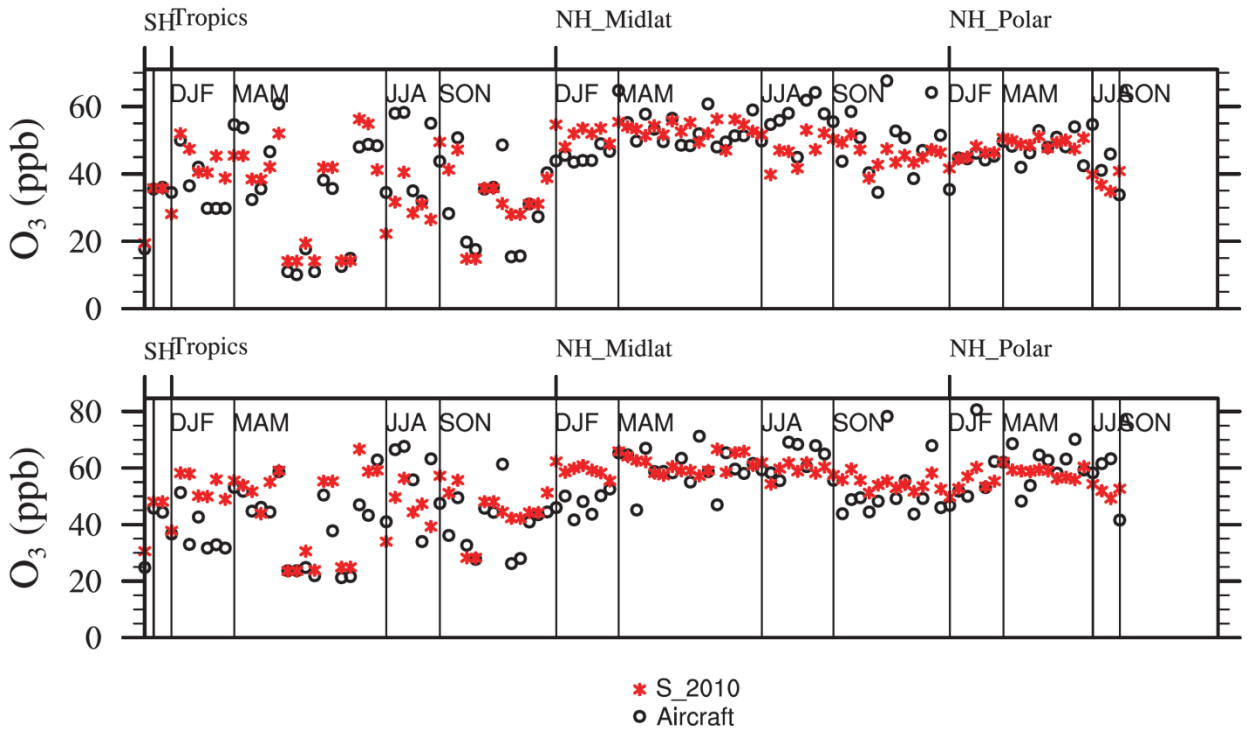

Figure 26. Comparisons of monthly mean O_3 from model output (red) with aircraft profiles (black, Table 9 as in ref. 40) at specific time periods and locations, for the four-year average S_2010 simulation, averaged over 0-3 km (top) and 2-7 km (bottom).

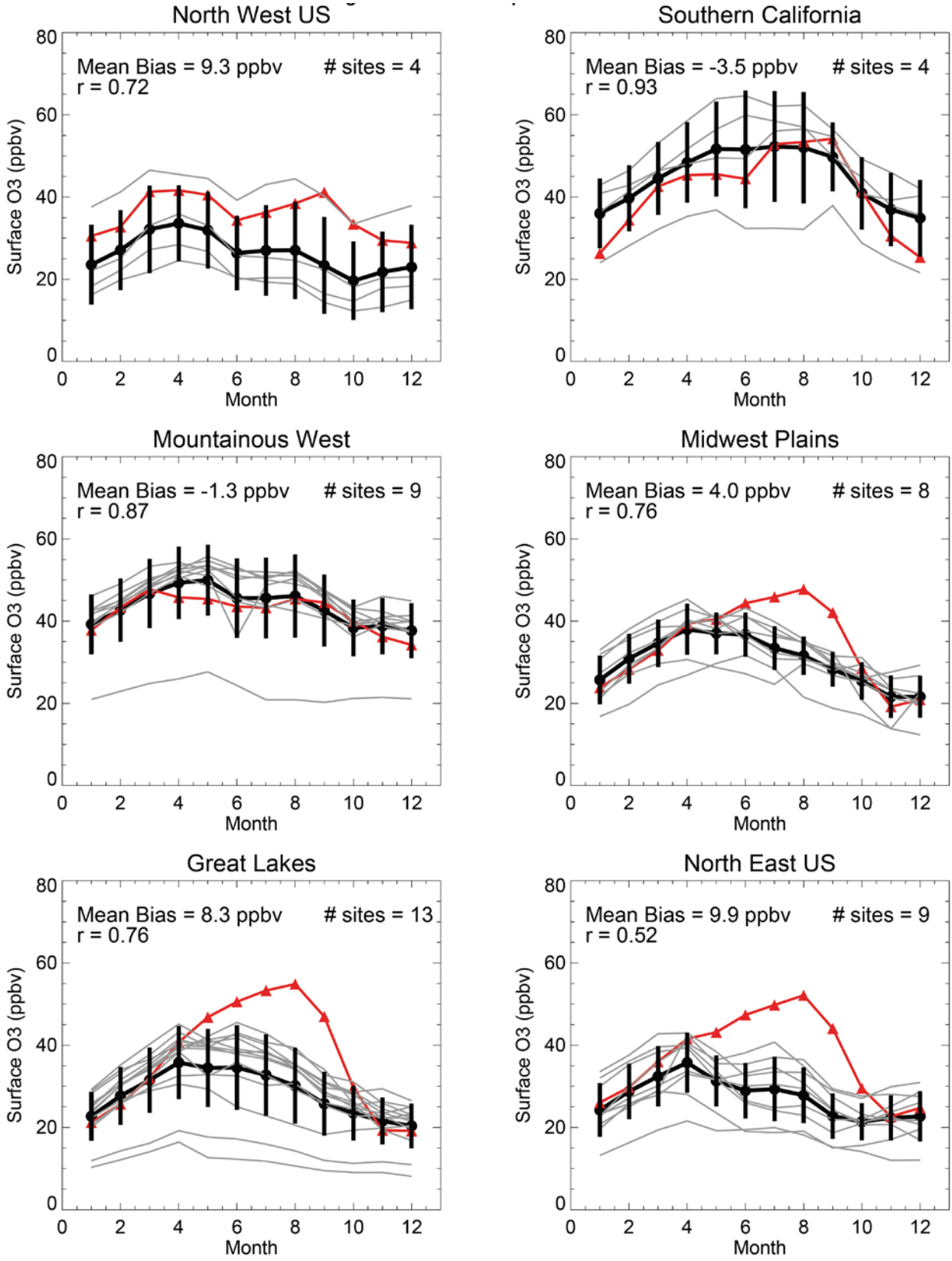
North West US
Mean Bias = 9.3 ppbv
r = 0.72
# sites = 4
Southern California
Mean Bias = -3.5 ppbv
r = 0.93
# sites = 4
Mountainous West
Mean Bias = -1.3 ppbv
r = 0.87
# sites = 9
Midwest Plains
Mean Bias = 4.0 ppbv
r = 0.76
# sites = 8
Great Lakes
Mean Bias = 8.3 ppbv
r = 0.76
# sites = 13
North East US
Mean Bias = 9.9 ppbv
r = 0.52
# sites = 9
Surface O3 (ppbv)
Month

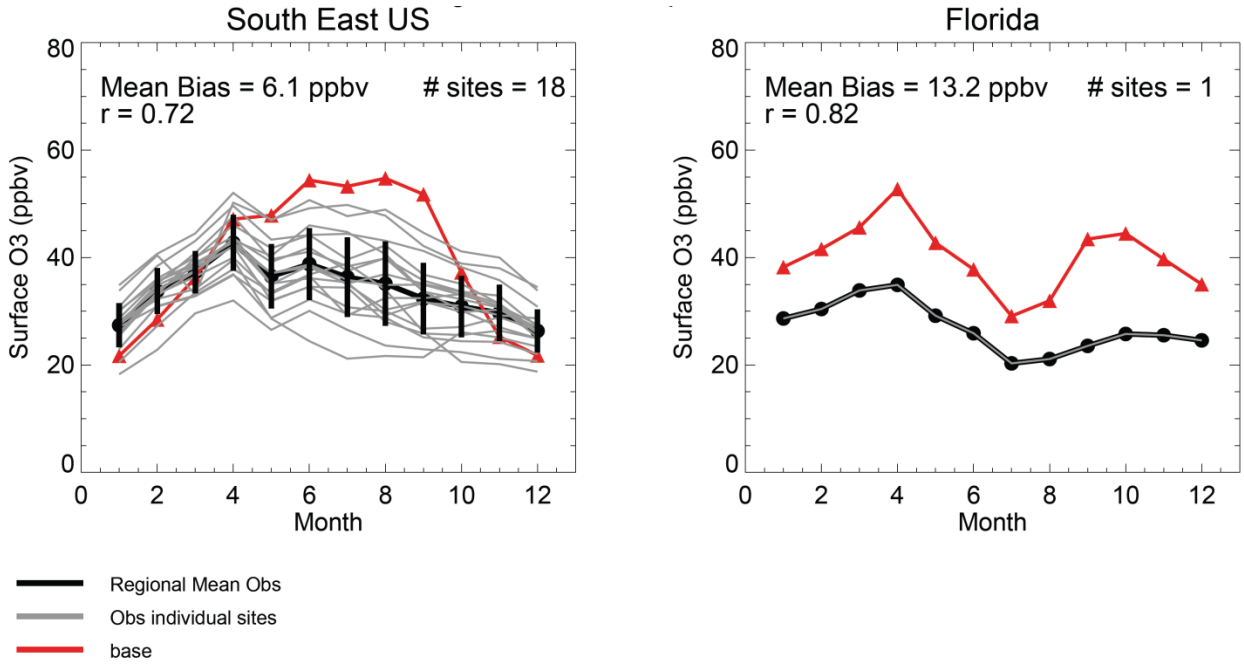

Figure 27. Comparison of four-year monthly average surface O_3 mixing ratios from the S_2010 simulation (red) with observations from the CASTNET monitoring network in the U.S. from 2009 to 2012, showing the CASTNET regional mean (black) and individual monitoring locations (grey). The overall mean bias over all measurement sites is 5.75 ppbv.

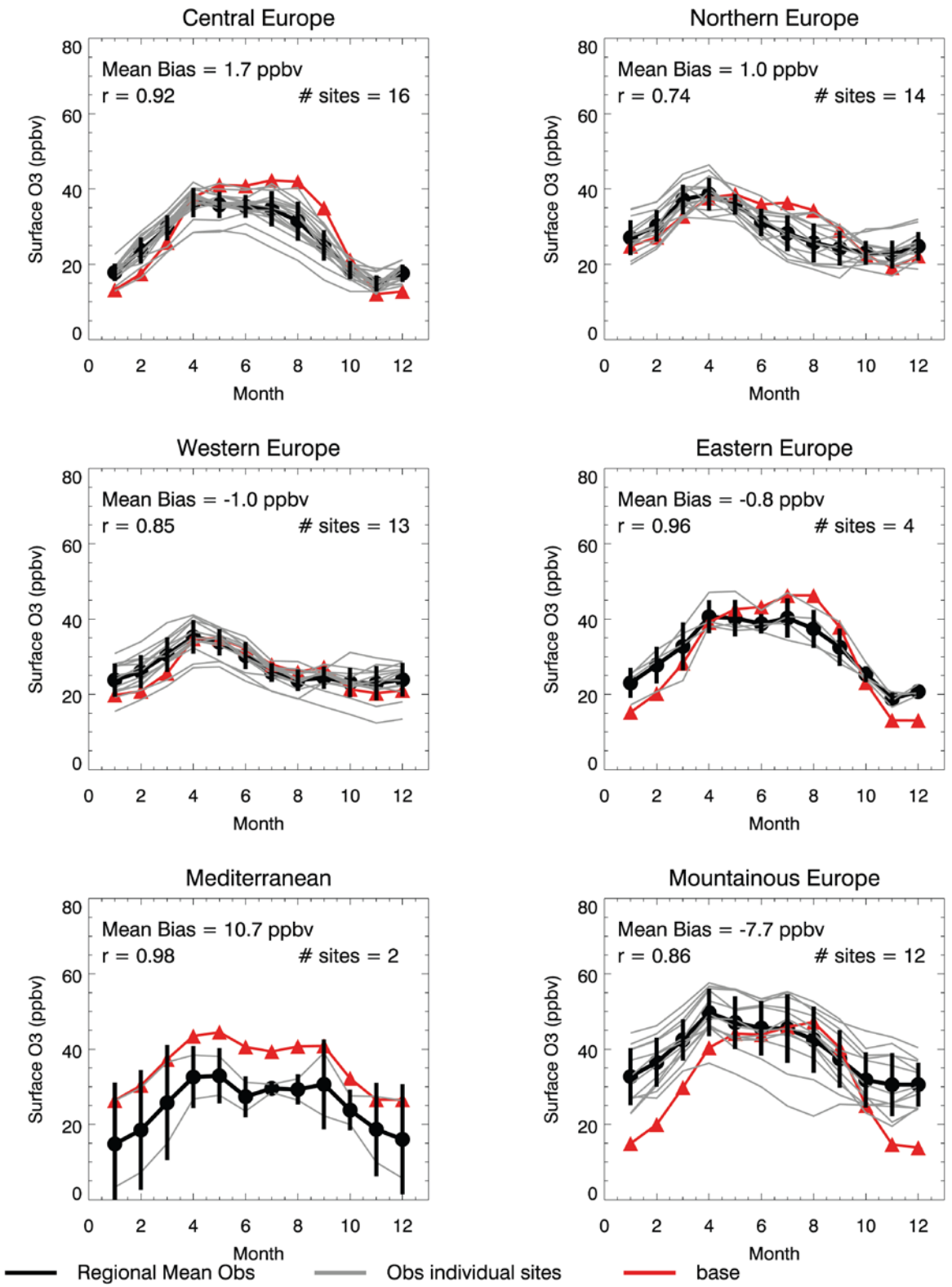

Figure 28. Comparison of four-year monthly average surface O_3 mixing ratios from the S_2010 simulation (red) with observations from the EMEP monitoring network in Europe from 2009-2011, showing the EMEP regional mean (black) and individual monitoring locations (grey). The overall mean bias over all measurement sites is 0.65 ppbv.

Table 1. Model simulations for this study. The last three are the sensitivity simulations described in the main paper.

	Emission total in year	**Spatial pattern in year**	**CH_4 concentration**
S_2010	2010	2010	1798 ppb
S_1980	1980	1980	1567 ppb
S_Distribution	2010	1980	1798 ppb
S_Magnitude	1980	2010	1798 ppb
S_CH_4	2010	2010	1567 ppb

Table 2. Interannual variability for the tropospheric O_3 burden change (ΔB_{O3}) from 1980 to 2010, for meteorological years 2009-2012 (unit Tg).

	4-year average	**Std**	**2009**	**2010**	**2011**	**2012**
Total change	28.12	0.93	26.58	29.04	28.65	28.22
Spatial pattern	16.39	0.83	15.08	17.38	16.69	16.43
Emission magnitude	8.59	0.22	8.42	8.34	8.84	8.78
Global CH_4	7.48	0.18	7.48	7.32	7.78	7.36

Table 3. The global tropospheric O_3 burden change (ΔB_{O3}) from 1980 to 2010 estimated by multiplying the change in NO_x emissions (the fifth column) in each of nine world regions by the sensitivity of B_{O3} per unit NO_x emissions (the second column) from a previous study[9]. The nine regions are defined as North America (NA), South America (SA), Europe (EU), Former Soviet Union (FSU), Africa (AF), India (IN), East Asia (EA), Southeast Asia (SE), and Australia and New Zealand (AU) (ref. 9). Notice that the total ΔB_{O3} calculated by this method (13.68 Tg) is much less than the values from our simulation, as we neglect changes in emissions of other species (VOCs, CO), and the sensitivities were calculated using a different model with different chemistry, meteorology, and base-year emissions for the early 1990s.

Regions	**$\Delta B_{O3}/\Delta E_{NOx}$ (Tg O_3 (TgN yr^{-1})$^{-1}$)**	**Emis_1980 (TgN yr^{-1})**	**Emis_2010 (TgN yr^{-1})**	**ΔEmis (TgN yr^{-1})**	**ΔB_{O3} (Tg O_3)**
NA	0.58	7.59	5.39	-2.20	-1.28
SA	3.25	1.74	2.24	0.50	1.62
EU	0.19	5.69	3.61	-2.08	-0.40
FSU	0.28	3.35	2.05	-1.31	-0.37
AF	1.21	5.39	7.23	1.85	2.23
IN	1.68	0.89	2.68	1.79	3.01
EA	0.62	2.99	8.34	5.35	3.32
SE	4.65	0.97	2.13	1.16	5.37
AU	3.14	0.75	0.80	0.05	0.17

Table 4. Percent change in tropospheric column ozone above three study regions as determined from OMI/MLS satellite retrievals (Figure 21) and in situ observations (IAGOS and SHADOZ, Figures 13-15). Statistically significant changes are in bold font, while insignificant changes are in italics.

	Change in the 1000-200 hPa ozone column from 1994-2004 until 2005-2014, as measured by IAGOS/SHADOZ	Change in the tropospheric ozone column (surface to tropopause) as detected by OMI/MLS, 2005-2015.
Southeast Asia		
DJF	**12%**	*4%*
MAM	**32%**	**13%**
JJA	**70%**	**19%**
SON	**45%**	**19%**
eastern China		
DJF	*4%*	**9%**
MAM	**8%**	*7%*
JJA	**15%**	**10%**
SON	**14%**	**8%**
southern India		
DJF	**12%**	*4%*
MAM	**25%**	**8%**
JJA	**20%**	**18%**
SON	**31%**	**18%**

Table 5. Long-term ozone observation sites used in this study (Figure 19).

Monitor sites	**Latitude/Longitude**	**Elevation (m)**
Barrow, US	71.1ºN /156.6 ºW	11
Hohenpeissenberg, Germany	47.8ºN/11.2ºE	975
Whiteface Mountain Summit, US	44.4ºN/73.9ºW	1484
Manua Loa, US	19.5ºN/155.6ºW	3397
Matatula Pt, Samoa	14.3ºS/170.6ºW	82
South Pole, Antarctica	90.0ºS/24.8ºW	2840

Table 6. Biases in the ozone burden (Tg) in the S_2010 simulation (four-year average) relative to OMI/MLS for the years 2009 to 2012 (S_2010 – OMI/MLS), corresponding to Figure 20.

	60°S-30°S	**30°S-0**	**0-30°N**	**30°N-60°N**	**Total**
ANN	-5.75	9.84	15.17	4.53	23.79
DJF	-8.82	4.36	25.05	8.92	29.51
MAM	-5.12	9.28	11.54	2.05	17.75
JJA	-1.39	20.11	9.63	-1.85	26.5
SON	-6.80	6.06	14.54	11.28	25.08

Table 7. Differences in the ozone burden (Tg) between S_2010 and S_1980 (four-year average). The total column is calculated for 60°S-60°N only, to be consistent with Table 6.

	60°S-30°S	**30°S-0**	**0-30°N**	**30°N-60°N**	**Total**
ANN	3.32	8.01	9.92	5.07	26.31
DJF	2.77	6.55	9.39	4.12	22.83
MAM	2.75	6.54	10.33	4.11	23.72
JJA	3.26	10.80	10.88	3.95	28.90
SON	3.73	10.88	11.75	5.18	31.55

Table 8. Locations of ozonesonde sites used in Figures 18, 23 and 24.

WMO code	Station	Latitude/Longitude	Data record
18	Alert	82ºN /62ºW	1995-2011
89	Ny Alesund	79ºN/12ºE	1995-2006
21	Edmonton	53ºN/114ºW	1995-2011
156	Payerne	47ºN/7ºE	1995-2011
12	Sapporo	43ºN/141ºE	1995-2009
190	Naha	26ºN/128ºE	1995-2008
434	San Cristobal	1°S/90°W	1998-2008
256	Lauder	45°S/170°E	1995-2008
644	Neumayer	71°S/8°W	1995-2011
99	Hohenpeissenberg	47.8°N/11.0°E	1966-2015
76	Goose Bay	53.3°N/60.3°W	1966-2015
107	Wallops Island	37.9°N/75.5°W	1971-2015

Table 9. Aircraft campaigns used in this study for model evaluation purposes (Figure 26)[40].

Campaign	Year	Month	Platform
TOTE	1995	December	DC-8
VOTE	1996	January	DC-8
STRAT	1995/96	Jan-Dec	ER-2
PEM-Trop-A	1996	Aug-Oct	P3/DC-8
SONEX	1997	Oct-Nov	DC-8
POLARIS	1997	Apr-Jun, Sep	ER-2
POLINAT-2	1997	Sep-Oct	Falkon
PEM-Trop-B	1999	Mar-Apr	P3/DC-8
ACCENT	1999	Apr, Sep-Oct	WB57
SOS	1999	Jun, Jul	NOAA WP-3D
SOLVE	99/00	Dec-Mar	DC-8
SOLVE	99/00	Dec-Mar	ER-2
TOPSE	2000	Feb-May	C130
TRACE-P	2000	Feb-Apr	P3/DC8
TexAQS	2000	Aug, Sep	NOAA WP-3D
ITCT	2002	Apr, May	NOAA WP-3D
Crystal Face	2002	Jun-Jul	WB57
INTEX-A	2004	Mar-Aug	DC8
NEAQS-ITCT	2004	Jul, Aug	NOAA WP-3D
Ave Fall	2004	Oct, Nov	WB57
Ave Houston	2005	June	WB57
Polar Ave	2005	Jan, Feb	WB57
Cr-Ave	2006	Jan, Feb	WB57
INTEX-B	2006	Mar-Aug	DC8
TexAQS	2006	Sep, Oct	NOAA WP-3D
TC4	2007	July	WB57
APCPAC	2008	Mar, Apr	NOAA WP-3D
APCTAS	2008	Apr-Jun	DC-8
START08	2008	Apr-Jun	G5
CalNex	2010	May, Jun	NOAA WP-3D

Review of global ozone trends, 1980-2010

Comprehensive observation-based assessments of global tropospheric ozone trends are difficult to produce due to the paucity of observations across large regions of the Earth. The most thorough assessment of global ozone trends, relying on all peer-reviewed studies, recently appeared in the Fifth IPCC Assessment Report (2013), with an update by Cooper et al[21]. Following are key excerpts from the Fifth IPCC Assessment Report (IPCC AR5) describing global ozone trends for the periods 1970-2010 and 1990-2010:

> "Satellite-based tropospheric column ozone retrievals across the tropics and mid-latitudes reveal a greater burden in the NH than in the SH. Tropospheric column ozone trend analyses are few. An analysis by Ziemke et al. (2005) found no trend over the tropical Pacific Ocean but significant positive trends (5 to 9% per decade) in the mid-latitude Pacific of both hemispheres during 1979 – 2003. Significant positive trends (2 to 9% per decade) were found across broad regions of the tropical South Atlantic, India, southern China, southeast Asia, Indonesia and the tropical regions downwind of China."

> "Long-term ozone trends at the surface and in the free troposphere can be assessed only from in situ measurements at a limited number of sites, leaving large areas such as the tropics and SH sparsely sampled. Nineteen predominantly rural surface sites or regions around the globe have long-term records that stretch back to the 1970s, and in two cases the 1950s. Thirteen of these sites are in the NH, and 11 sites have statistically significant positive trends of 1 to 5 ppb per decade, corresponding to >100% ozone increases since the 1950s and 9 to 55% ozone increases since the 1970s. In the SH, three of six sites have significant trends of approximately 2 ppb per decade and three have insignificant trends. Free tropospheric monitoring since the 1970s is more limited. Significant positive trends since 1971 have been observed using ozonesondes above Western Europe, Japan and coastal Antarctica (rates of increase range from 1 to 3 ppb per decade), but not at all levels. In addition, aircraft have measured significant upper tropospheric trends in one or more seasons above the north-eastern USA, the North Atlantic Ocean, Europe, the Middle East, northern India, southern China and Japan. Insignificant free tropospheric trends were found above the Mid-Atlantic USA (1971–2010) and in the upper troposphere above the western USA (1975–2001). No site or region showed a significant negative trend."

> "In recent decades ozone precursor emissions have decreased in Europe and North America and increased in Asia, impacting ozone production on regional and hemispheric scales. Accordingly, 1990 – 2010 surface ozone trends vary regionally. In Europe ozone generally increased through much of the 1990s but since 2000 ozone has either levelled off or decreased at rural and mountaintop sites, as well as for baseline ozone coming ashore at Mace Head, Ireland. In North America surface ozone has increased in eastern and Arctic Canada, but is unchanged in central and western Canada. Surface ozone has increased in baseline air masses coming ashore along the west coast of the USA and at half of the rural sites in the western USA during spring. In the eastern USA surface ozone has decreased strongly in summer, is largely unchanged in spring and has increased in winter. East Asian surface ozone is generally increasing and at downwind sites ozone is increasing at Mauna Loa, Hawaii but decreasing at

Minami Tori Shima in the subtropical western North Pacific. In the SH ozone has increased at the eight available sites, although trends are insignificant at four sites. Owing to methodological changes, free tropospheric ozone observations are most reliable since the mid-1990s. Ozone has decreased above Europe since 1998 and is largely unchanged above Japan. Otherwise the remaining regions with measurements (North America, North Pacific Ocean, SH) show a range of positive trends (both significant and insignificant) depending on altitude, with no site having a negative trend at any altitude."

"In summary, there is medium confidence from limited measurements in the late 19th through mid-20th century that European surface ozone more than doubled by the end of the 20th century. There is medium confidence from more widespread measurements beginning in the 1970s that surface ozone has increased at most (non-urban) sites in the NH (1 to 5 ppb per decade), while there is low confidence for ozone increases (2 ppb per decade) in the SH. Since 1990 surface ozone has likely increased in East Asia, while surface ozone in the eastern USA and Western Europe has levelled off or is decreasing. Ozone monitoring in the free troposphere since the 1970s is very limited and indicates a weaker rate of increase than at the surface. Satellite instruments can now quantify the present-day tropospheric ozone burden on a near-global basis; significant tropospheric ozone column increases were observed over extended tropical regions of southern Asia, as well as mid-latitude regions of the South and North Pacific Ocean since 1979."

The electronic supplement to IPCC AR5 contains a figure and table (Figure 2.SM.1, Table 2.SM.2) summarizing ozone trends for the period 1980-2010 (Hartmann et al., 2013). Trends during this time are consistent with the 1970-2010 trends except for some decreases at sites in central and northern North America.

Since the publication of IPCC AR5 three new studies demonstrate the continuing increase of surface ozone in China and South Korea. In China ozone increased significantly at the Mt Waliguan (36.28° N, 100.9° E, 3816 m a.s.l.) high elevation rural monitoring site in western China at the rate of 0.25 ± 0.17 ppbv yr^{-1} during 1994-2013 (Xu et al., 2016). In addition, ozone has been observed during summertime at Mt Tai (36.25° N, 117.10° E, 1534 m a.s.l.) in the North China Plain from 2003-2015. Ozone has increased at the rate of 1.7 ± 1.0 ppbv yr^{-1} during June and 2.1 ± 0.9 ppbv yr^{-1} during July-August (Sun et al., 2016). In South Korea ozone increased across the country (56 surface sites, mostly urban) at the rate of 0.48 ± 0.07 ppbv yr^{-1} during 1990-2010.

Focusing on the free troposphere above South and East Asia, observations of free tropospheric ozone trends are very limited, however significant positive trends were observed in various layers above the mid-latitude Japanese sites of Sapporo and Tsukuba (1981-2010) and the subtropical site of Naha, Japan (1991-2010), with no layer showing a significant decrease (Oltmans et al., 2013).

To expand our understanding of Asian free tropospheric ozone trends we conducted an additional analysis for this manuscript using 20 years (1994-2014) of IAGOS (http://www.iagos.org/; Petzold et al., 2015; Nedelec et al., 2015) commercial aircraft ozone profiles above Southeast Asia (Figure 13), northeastern China (Figure 14), and southern India (Figure 15). The Southeast Asia trend analysis also included 11 years (2004-2014) of ozonesonde profiles above Hanoi, Vietnam, provided by the NASA SHADOZ program (Thompson et al., 2003): http://croc.gsfc.nasa.gov/shadoz/. Due to insufficient observations

over these regions between 1980 and 1993, this analysis has to begin in 1994. IAGOS aircraft have not flown to these regions consistently since 1994, with heavy sampling in some years and no sampling in others. Therefore to ensure robust sample sizes the analysis is limited to quantifying the changes in ozone from the period 1994-2004 until the period 2005-2014.

Above Southeast Asia ozone increased significantly at all levels from the surface to 200 hPa during spring, summer and autumn. During winter significant increases only occurred in the mid- and upper troposphere. Maximum increases were as high as 20 ppbv for median values and 40 ppbv for the 95th percentile. Above northeastern China ozone increased significantly at virtually all levels during spring, summer and autumn and in the mid-troposphere during winter. Above southern India significant increases were found at all levels during spring and autumn and in the lower and upper troposphere during winter and summer. Other available Asian data sets, such as IAGOS profiles above northern India or the Middle East, are too sparse to allow robust calculations of ozone trends. Maximum increases were as high as 20 ppbv for median values and 35 ppbv for the 95th percentile. This analysis of free tropospheric ozone trends at mid- and low latitudes above south and east Asia is all that can be achieved with the available in situ observations. Other available data sets, such as IAGOS profiles above India, are too sparse to allow robust calculations of ozone trends. This observation-based analysis is important in that it demonstrates, for the first time, that ozone in the free troposphere has increased significantly over southern India and southeast Asia during the past 20 years. With regards to northeastern China, our analysis extends the original 1994-2005 analysis of Ding et al.[24], to show that the positive trend they detected has continued through 2014.

The only other continuous data set available for assessing decadal changes in tropospheric ozone over low latitudes is the OMI/MLS tropospheric column ozone product, derived from the Ozone Monitoring Instrument (OMI) and Microwave Limb Sounder (MLS) remote sensors onboard NASA's polar orbiting Aura satellite (Ziemke et al. 2006). This near-global ozone record, now greater than 11 years (2004-2015), is shown in Figure 21. On an annual basis the greatest tropospheric column ozone values are found above the eastern Mediterranean, the Arabian Sea and northeastern China. Ozone increased significantly in a broad swath across the tropics and subtropics, stretching from western South America eastwards to Africa and the western Pacific Ocean. The strongest trends are found above south and southeastern Asia.

While this 2004-2015 satellite product does not match the 1980-2010 study period of this study, it does indicate that ozone has increased at low latitudes and across broad regions of South and East Asia where emissions of ozone precursor gases have also increased. The satellite observed increases over 2005-2015 are broadly consistent with the in situ trends detected by the IAGOS/SHADOZ profiles (1994-2004 to 2005-2015) with the 10-year satellite-detected increase being less than the 20-year increase detected by the in situ observations (Table 4).

Hartmann, D.L., A.M.G. Klein Tank, M. Rusticucci, L. Alexander, S. Brönnimann, Y. Charabi, F. Dentener, E. Dlugokencky, D. Easterling, A. Kaplan, B. Soden, P. Thorne, M. Wild and P.M. Zhai, 2013: Observations: Atmosphere and Surface Supplementary Material. In: Climate Change 2013: The Physical Science Basis. Contribution of Working Group I to the Fifth Assessment Report of the Intergovernmental Panel on Climate Change [Stocker, T.F., D. Qin, G.-K. Plattner, M. Tignor, S.K. Allen, J. Boschung, A. Nauels, Y. Xia, V. Bex and P.M. Midgley (eds.)]. Available from www.climatechange2013.org and www.ipcc.ch.

IPCC (2013), Climate Change 2013: The Physical Science Basis. Contribution of Working Group I to the Fifth Assessment Report of the Intergovernmental Panel on Climate Change [Stocker, T.F., D. Qin, G.-K. Plattner, M. Tignor, S.K. Allen, J. Boschung, A. Nauels, Y. Xia, V. Bex and P.M. Midgley (eds.)]. Cambridge University Press, Cambridge, United Kingdom and New York, NY, USA, 1535 pp.

Lee, H. J. *et al.* Transport of NOx in East Asia identified by satellite and in situ measurements and Lagrangian particle dispersion model simulations. *J. Geophys. Res.* **119,** 2574–2596 (2014).

Liu, S. C. *et al.* Ozone production in the rural troposphere and the implications for regional and global ozone distributions. *J. Geophys. Res.* **92,** 4191–4207 (1987).

Nedelec, P. *et al.* Instrumentation on commercial aircraft for monitoring the atmospheric composition on a global scale: the IAGOS system, technical overview of ozone and carbon monoxide measurements, *Tellus B*, **67**, 27791 (2015).

Oltmans, S. J. et al. Recent tropospheric ozone changes – A pattern dominated by slow or no growth, *Atmos. Env.*, **67**: 331-351 (2013).

Petzold, A. *et al.* Global-scale atmosphere monitoring by in-service aircraft – current achievements and future prospects of the European Research Infrastructure IAGOS, *Tellus B*, **67**: 28452 (2015).

Sillman, S., He, D., Cardelino, C. & Imhoff, R. E. The use of photochemical indicators to evaluate ozone-NO_x-hydrocarbon sensitivity: Case studies from Atlanta, New York, and Los Angeles. *J. Air Waste Manag. Assoc.* **47,** 1030–1040 (1997).

Sun, L., Xue, L., Wang, T., Gao, J., Ding, A., Cooper, O. R., Xu, P., Wang, Z., Wang, X., Wen, L., Zhu, Y., Chen, T., Yang, L., Wang, Y., Chen, J., and Wang, W.: Significant increase of summertime ozone at Mt. Tai in Central Eastern China: 2003–2015, Atmos. Chem. Phys. Discuss., doi:10.5194/acp-2016-220, in review, 2016.

Thompson, A.M. *et al.* Southern Hemisphere Additional Ozonesondes (SHADOZ) 1998-2000 tropical ozone climatology 1. Comparison with Total Ozone Mapping Spectrometer (TOMS) and ground-based measurements, *J. Geophys. Res.*, **108**, D2, 8238 (2003).

Xu, W., Lin, W., Xu, X., Tang, J., Huang, J., Wu, H., and Zhang, X.: Long-term trends of surface ozone and its influencing factors at the Mt Waliguan GAW station, China – Part 1: Overall trends and characteristics, *Atmos. Chem. Phys.*, **16**, 6191-6205 (2016).

Ziemke, J. R., S. Chandra, B. N. Duncan, L. Froidevaux, P. K. Bhartia, P. F. Levelt, and J. W. Waters. Tropospheric ozone determined from Aura OMI and MLS: Evaluation of measurements and comparison with the Global Modeling Initiative's Chemical Transport Model, *J. Geophys. Res.*, **111**, D19303 (2006).